PLASMACHEMICAL SYNTHESIS OF CARBON SUBOXIDE

A Thesis

by

ROBERT PAUL GEIGER

Submitted to the Office of Graduate Studies of
Texas A&M University
in partial fulfillment of the requirement for the degree of

MASTER OF SCIENCE

Approved by:

Chair of Committee,	David Staack
Committee Members,	Nicole Zacharia
	Sergio Capareda
Head of Department,	Jerry Caton

May 2013

Major Subject: Mechanical Engineering

ABSTRACT

A nonthermal carbon monoxide plasma is known to produce a solid deposition which is thought to be a polymer of carbon suboxide (C_3O_2); however there are very few investigations of this deposition in the literature. This thesis contains an analysis of the theoretical thermodynamics and kinetics of carbon suboxide formation as well as experimental results. The theoretical analysis suggests that carbon suboxide may be an equilibrium product even at ambient conditions but favors lower temperatures; furthermore if solid carbon is considered to be kinetically limited, and therefore not a product, then carbon suboxide is more likely to be a product under these pseudo-equilibrium conditions. Experimentally, solid films were produced in a dielectric barrier discharge (DBD) containing pure carbon monoxide. Optical emission spectroscopy was used to analyze the plasma and models of the emission spectra were created to determine the plasma temperatures. Deposition rates were determined to be on the order of 0.2 mg/min at a power of about 10W; it is expected however that these conditions are not optimized. The overall kinetics of carbon suboxide was analyzed and optimal conditions for operation can be estimated. Characterization of the solid depositions were carried out using Solid State Nuclear Magnetic Resonance (NMR), Fourier Transform Infrared Spectroscopy (FTIR), Electrospray Ionization Mass Spectroscopy (ESI-MS), and Matrix-assisted Laser Desorption Ionization Mass Spectroscopy (MALDI-MS). The characteristics of the film are very comparable to hydrolyzed carbon suboxide polymer suggesting that carbon suboxide polymer were in fact created in the carbon monoxide plasma at atmospheric conditions.

ACKNOWLEDGEMENTS

First and foremost I must express my sincerest gratitude to my undergraduate research advisors Dr. Alexander Fridman and Dr. Alexander Gutsol of the Drexel Plasma Institute. It was their brilliance and enthusiasm towards new and radical research that first introduced me to the research that is the topic of this thesis. If it were not for them this research would not exist.

Concurrently responsible for the initiation and completion of this work, my graduate advisor Dr. David Staack shared the excitement and interest in this work and greatly encouraged me to pursue this research. It was largely his knowledge and motivation that led to the successes we had throughout this research. For that and for his overall support I am eternally grateful.

TABLE OF CONTENTS

Page

ABSTRACT ii

ACKNOWLEDGEMENTS iii

TABLE OF CONTENTS iv

LIST OF TABLES vi

LIST OF FIGURES vii

1. INTRODUCTION 1

1.1 Background 1
1.2 History of Carbon Suboxide 3
1.3 Prospects for Industrial Application 5
1.4 Introduction to Nonthermal Plasma-chemistry 10
1.4.1 Plasma Physics 10
1.4.2 Catalysis and Plasma 11
1.4.3 The Dielectric Barrier Discharge 13
1.5 Thesis Objectives 14

2. THERMODYNAMICS AND KINETICS OF CARBON SUBOXIDE 16

2.1 Thermodynamic Properties 16
2.2 Equilibrium States of Oxides of Carbon 26
2.3 Kinetics of Carbon Suboxide Formation from Carbon Monoxide 30

3. EXPERIMENTAL DESIGN 40

3.1 Carbon Monoxide Safety 40
3.2 General Setup 41
3.3 Reactor Design 42
3.4 Power Measurements 44

4. EXPERIMENTAL RESULTS 45

4.1 Plasma Parameters 45
4.2 Overall Kinetics 49
4.3 Characterization 56

Page

5. CONCLUSIONS AND FUTURE WORK 68

5.1 Summary 68
5.2 Work Accomplished 68
5.3 Major Findings 69
5.4 Conclusions 69
5.5 Suggested Future Work 70

REFERENCES 73

APPENDIX 83

LIST OF TABLES

Page

Table 1 Thermodynamic properties of carbon suboxide monomer and polymerized carbon suboxide 17

Table 2 Shomate coefficients for carbon suboxide monomer. 18

Table 3 Joback method results for carbon suboxide 21

Table 4 Joback groub contributions used for carbon suboxide 22

Table 5 Equations considered for the thermodynamic equilibrium calculations 27

Table 6 Reaction and standard pressure and temperature reaction rates leading to solid carbon and carbon suboxide formation from carbon monoxide 32

Table 7 Mechanism of carbon suboxide formation in nonthermal plasma with Te = 1 eV 39

Table 8 Composition as determined by XPS 58

LIST OF FIGURES

Page

Figure 1 The induction tube of W. Siemens [37] 4

Figure 2 Conceptual flow chart of hydrocarbon utilization incorporating carbon suboxide 6

Figure 3 Possible products using a carbon suboxide precursor 8

Figure 4 Schematic of Dielectric Barrier Discharge (DBD) 14

Figure 5 Entropy of carbon suboxide monomer in the gas phase verses temperature 19

Figure 6 Enthalpy of carbon suboxide in the gas phase verses temperature 20

Figure 7 Specific heat of carbon suboxide in the gas phase verse temperature 20

Figure 8 P-v diagram of carbon suboxide 25

Figure 9 P-T diagram for carbon suboxide 26

Figure 10 Enthalpy of vaporization of carbon suboxide as a function of temperature 26

Figure 11 Thermodynamic equilibrium calculations for various temperatures considering only the following: 28

Figure 12 The rate of formation of solid carbon suboxide polymer relative to the rate of formation of solid carbon if plotted verse initial gaseous carbon concentration relative to the initial carbon monoxide concentration at a constant temperature of 300K 33

Figure 13 Relative reaction rates for formation of carbon suboxide relative to solid carbon as a function of temperature at [C]/[CO] = 3. 10E-04. 33

Figure 14 Rate coefficients for the electron impact dissociation of O_2 (k_1), CO (k_2), and CO_2 (k_3) [81] 35

Figure 15 Reaction coefficients for the dissociation of carbon monoxide by electron impact extrapolated from the data provided by Cosby [83]. 36

Figure 16 Schematic of Experimental Setup indicating gas and electrical flows 42

Figure 17 Experimental DBD reactor 43

Figure 18 Voltage and current characteristics of the discharge 44

Page

Figure 19 An illustration of the excited states of carbon monoxide that were modeled. The red arrow indicates the most probable transition according to the Franck-Condon principal. The dotted indicates the dissociation energy of carbon monoxide from its ground state..... 47

Figure 20 a) Experimental optical emission spectrum of the DBD carbon monoxide plasma b) Model of Angstrom CO Bands c) Model of Herzberg CO Bands and d) Model of C_2 Swan Bands *Note: The models (b,c,d) shown were calculated at Tvib = 1200K and Trot = 400K*..... 48

Figure 21 C_2 Swan Band C_2 ($d^3\Pi$-$a^3\Pi$) fit to the experimental data at the 2-1 and 1-0 transitions. 48

Figure 22 Rate of deposition plotted verse time a power of 10W and a flow rate of 0. 5 SLPM..... 50

Figure 23 Deposition rate plotted verse flow rate 51

Figure 24 Deposition rate plotted verse power at 0. 5 SLPM for 10 minute runs. 52

Figure 25 Gas temperature leaving the plasma verses time for various powers 53

Figure 26 a) Variance of film color within the DBD. b) Comsol model of the flow within the DBD assuming uniform heating of Q = 500 W/m^3 55

Figure 27 Figure 28 a) Picture of CO plasma from a side view b) Intensity plot of picture..... 56

Figure 29 XPS of yellow solid product..... 58

Figure 30 Visual comparison of A) Solid sample before being put into solution B) Solid sample after being put into an aqueous solution 59

Figure 31 XPS results for solid products before (Non-Hydrolyzed Powder) and after (Hydrolyzed Powder) the solid products were put into an aqueous solution 60

Figure 32 Solid State ^{13}C-MAS NMR of solid deposition: A) CPMAS B) H decoupling 64

Figure 33 FTIR of brown and yellow films 66

Figure 34 a) ESI + Mass Spectrum analysis showing multiply charged species around 1933.6 amu. B) Maldi Mass Spectrum analysis showing small molecular weights but no species up to 10000 amu..... 67

1. INTRODUCTION*

1.1 Background

Carbon suboxide has a fascinating history and the molecule has been explored by several prominent scientists such as Otto Paul Hermann Diels [1], Paul Harteck [2-8], Sir Benjamin Collins Brodie [9-11], Linus Pauling [12, 13] and Irving Langmuir [14, 15]. The molecule was once thought to be responsible for the red color seen on mars [16-19] and the yellow color in Venus clouds [20, 21] and it has been identified in the tail of Halley's Comet [22, 23]. It has been suggested that carbon suboxide played an important role in the primordial soup from which life first originated [24-26] and has been shown to be a precursor in the formation of amino acids [24, 26, 27]. The molecule itself has an interesting linear structure similar to carbon dioxide and can form polymers with interesting properties [28, 29]. All of these discoveries illustrate the possibility that the carbon suboxide molecule has an important role in the chemistry between oxygen and carbon.

The chemistry that occurs between carbon and oxygen plays a vital role to many of many natural processes of life, such as the carbon or oxygen cycles and the Krebs cycle, and in many man made industrial processes such as combustion and other oxidation processes. Predominantly carbon dioxide and carbon monoxide are the only pure oxides of carbon that are considered however the role of the other oxides of carbon, in particular carbon suboxide and dicarbon monoxide, may have subtle but important mechanistic roles [30-33]. Learning more about the characteristics and chemistry of these molecules may contribute to the overall

* Part of the data reported in this chapter is reprinted with permission from Geiger, R., Staack, D., *Analysis of Solid Products Formed in Atmospheric Non-thermal Carbon Monoxide Plasma* Journal of Physics D: Applied Physics, 2011. **44**(27) by IOP Publishing Ltd

understanding of the chemistry that occurs between carbon and oxygen and is a fundamental motivation that drives the research presented in this thesis.

Aside from intellectual curiosity there are many practical motivations for this research. Dr. Alexander Fridman and Dr. Alexander Gutsol developed the idea that plasma assisted low temperature oxidation of hydrocarbons may lead to hydrogen production with the major other product consisting of carbon suboxide. Because this process would not emit carbon dioxide, CO_2, and the final products for be solid carbon suboxide, C_3O_2, and hydrogen, H_2 there are obvious benefits to such a technology. A more thorough explanation of this concept was presented in a paper they wrote in 2006 entitled, 'CO_2-Free Energy and Hydrogen Production from Hydrocarbons' [34]. Related to this idea is the possibility of converting synthesis gas, consisting mainly of carbon monoxide and hydrogen, to liquid fuels and other solid products similar to the Fischer Tropsch process. Synthesis gas production is common in industry however the Fischer Tropsch process is not as common; it is energy intensive and can have the common issue of catalyst poisoning. Synthesis gas can alternatively be processed using nonthermal plasma. In this case it may be important to understand the mechanisms of pure carbon monoxide plasma in order to accurately interpret the results of synthesis gas processing; carbon suboxide and dicarbon monoxide may have important roles. Besides producing such value-added products as liquid fuels, carbon suboxide itself may be considered a value-added product that is desirable for various applications and this should be considered in more detail.

A review of the literature regarding carbon suboxide suggests that it was first formed by Brodie with the aid of a Siemens induction tube; and the only gas that he used was carbon monoxide. While considering the possible kinetics of such a process one might soon realize that

this process is a perfect example of an application for the non-equilibrium properties obtained from nonthermal plasma chemistry as will be explained further within this thesis.

1.2 History of Carbon Suboxide

Carbon Suboxide (C_3O_2) is one of the less well known oxides of carbon. It is a linear molecule comprised of four consecutive double bonds (O=C=C=C=O). Referred to as the first bisketene, it has the ability to form ladder polymers with interesting paramagnetic properties [29] the structure of which has recently been determined to have an α–pyrone structure [35]. According to the literature it would appear that carbon suboxide was first synthesized by Sir Benjamin C. Brodie.

In 1871 Brodie published the first of three papers describing experiments on electrified gas [36]. The setup consisted of a Siemens induction tube that was driven by a Ruhmkorff's coil. The Siemens induction tube is similar to the modern day dielectric barrier discharge (DBD). It consists of a glass tube within another glass tube as seen in Figure 1 [37]. The inner tube is filled with water and acts as one electrode while the outer tube is surrounded by water acting as the other electrode. When the voltage is applied to the electrodes, plasma is generated in the gap between the inner glass tube and the outer glass tube. The Ruhmkorff coil is an induction coil that resembles a transformer where the primary is driven by a low-voltage DC signal that is continually interrupted by a mechanical vibrating contact. The interruptions in the primary induce a high voltage pulse in the secondary which can be used to drive the previously described inductions tube. Modern day DBD discharges differ in that they are commonly driven by an AC signal instead of a pulsed DC. Within the papers that he published regarding plasma gas treatments Brodie mentions that he encountered a solid depositions formed on the wall of the

induction tube while passing carbon monoxide through it [10]. The solids had a red-brown color and were soluble in water creating a highly acidic solution. He noted that the samples he produced varied in composition from one experiment to the next. The variation in the compositions were limited to a certain number of forms; that is to say that they were always multiples of $C(CO)_n$. Brodie related these multiples to the well-known multiples of hydrocarbons $(CH_2)_n$. Brodie's 'oxycarbon' hypothesis would later prove to not be completely accurate.

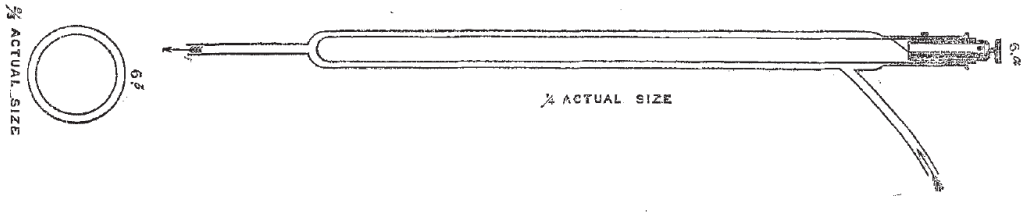

Figure 1 The induction tube of W. Siemens [37]

In 1906 and 1907 Diels reported a way to synthesize carbon suboxide by completely dehydrating malonic acid with phosphorous pentoxide [1]. The similarity between the polymers formed by Brodie and Diels fascinated Diels, however he was unable to determine whether they had produced the same material. Eventually Lunt and Mumford in the late 1920's investigated it further and determined that although carbon suboxide monomer was produced in the plasma the polymer created differed from that of Diels [38-40]. They believed the main difference was that Brodies method produced excess carbon in the polymer film due to pyrolysis and due to reaction with water. It is apparent from the papers published by Lunt and others that the reactive nature of the carbon suboxide polymers makes it very difficult to accurately analyze the solid products

formed in the plasma; however it was demonstrated by Ott that carbon suboxide monomer is produced to a small extent [41].

Since its initial discovery carbon suboxide has made appearances in literature regarding carbon dioxide cooled nuclear reactors [42], carbon monoxide lasers [43], and more recently in extremely high pressure carbon monoxide [44-49]. The photochemistry of carbon monoxide was investigated and described by several authors; it was determined that carbon monoxide, when excited to the $a^3\Pi$ state (Cameron Bands) it would react to produce carbon dioxide and carbon suboxide, both in the gas phase and the polymerized solid phase [6]. It was determined that excited CO must play an important role in the production of carbon suboxide [50] and the mechanism of formation was determined to proceed through dicarbon monoxide. Furthermore the production of suboxide was again noted to be very sensitive to humidity and would produce methanol and formaldehyde. Lastly, carbon monoxide, when take to very high pressure, also demonstrated a phase change to a yellow film, which is stable at atmospheric pressure, having remarkable similarities to carbon suboxide [44-49].

1.3 Prospects for Industrial Application

There is some renewed interest in carbon suboxide in relation to carbon dioxide sequestration and utilization methods and considering the growing concerns about climate change. One possibility is the sequestration of carbon dioxide as a suboxide polymer. It has been shown that carbon dioxide dissociation to carbon monoxide using a plasma process can have efficiencies reaching as high as 90% [51], while further processing may efficiently produce suboxide polymers; it is necessary to first produce carbon monoxide as the precursor for suboxide polymer formation. While this process is certainly energy intensive it may be comparable to other sequestration technologies with the added benefit of actually converting the

carbon dioxide to a solid material. It may also be worth considering extracting carbon monoxide from syngas produced from partial oxidation to avoid complete combustion which would reduce energy costs. The process of sequestering oxidized carbon as a carbon oxide polymer may have certain advantages over other sequestration methods such as producing value-added products and carbon dioxide utilization. The plasma technology necessary is already being incorporated in industry for the efficient production of ozone [52]. Very similar reactors can be created and optimized for carbon suboxide production using a carbon monoxide feed gas.

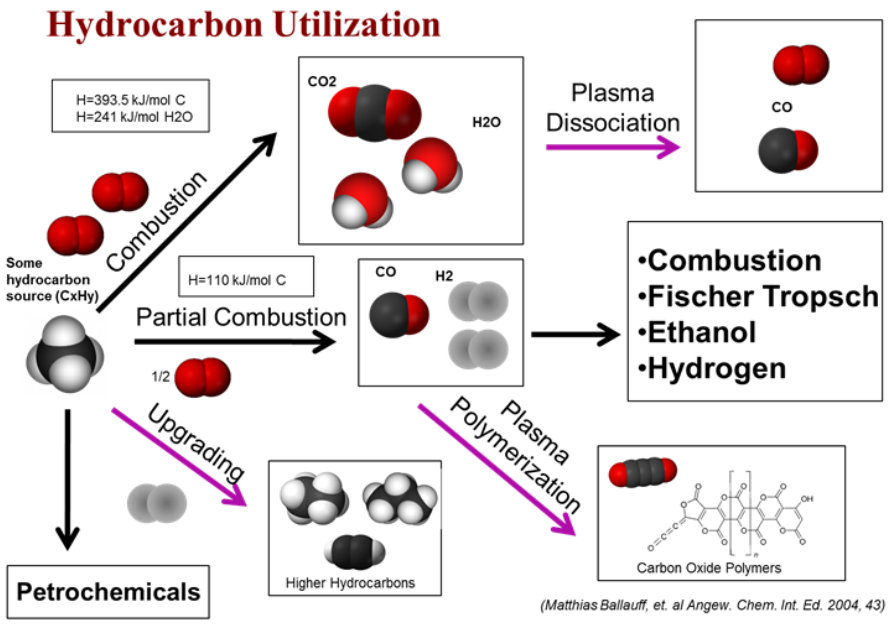

Figure 2 Conceptual flow chart of hydrocarbon utilization incorporating carbon suboxide

The idea of converting hydrocarbons directly to carbon suboxide polymers and hydrogen has also been suggested [34]. This method of carbon suboxide production provides an interesting clean energy alternative for the utilization of hydrocarbon by CO_2 free combustion, however this

direct conversion technology is rather complex if coal, oil, biomass or even methane are to be used. For such a technology to be developed it would be beneficial to further understand the mechanisms for the known methods of forming carbon suboxide, such as what is being presented here. As illustrated in Figure 2 the hydrocarbon utilization process in general begins with some hydrocarbon source, most likely a source that is currently of low value such as biomass or coal, which is processed further either by complete combustion, partial combustion or upgrading. Each of these processes is capable of either producing energy or some other more valuable resource. The production of carbon dioxide through complete combustion is also the most exothermic of all the processes and is often the most desirable reaction is energy production is the main goal; however the carbon dioxide product is generally of little value and often exhausted into the atmosphere. The exhausting of carbon dioxide into the atmosphere has been suggested as being detrimental to the atmosphere and therefore alternative processes are being sought. The dissociation of carbon dioxide using plasma has been investigated and very high efficiencies are quite well known, however this is still a very energy intensive process and is therefore unlikely to be incorporated with a combustion process. Hydrocarbon upgrading, that is taking a small hydrocarbon and upgrading it to a higher hydrocarbon, is also known to be possible using plasma technologies. A new possibility that is shown in Figure 2 is producing carbon suboxide from the synthesis gas products of partial combustion. Such a process can produce some energy, hydrogen, and the value added products of carbon suboxide. Such a process may prove to be economically viable if the appropriate products are produced.

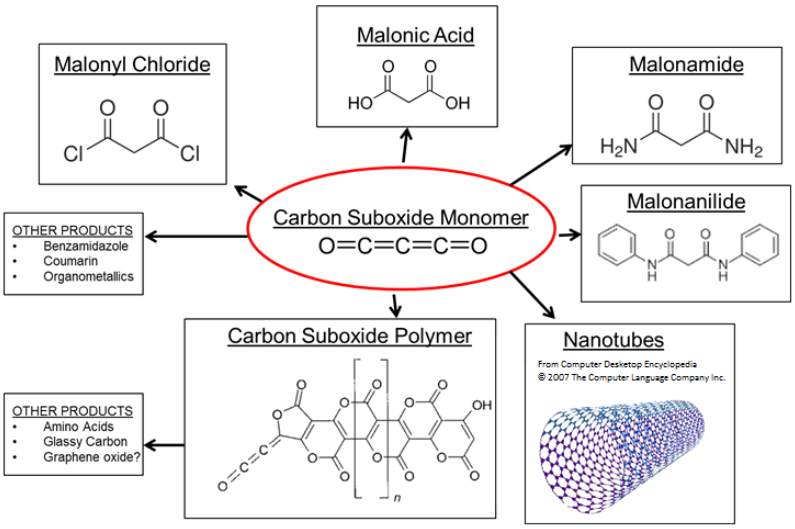

Figure 3 Possible products using a carbon suboxide precursor

The potential for industrial carbon suboxide utilization is great but yet unrealized and some of the valuable products that can be produced using carbon suboxide as a precursor are illustrated in Figure 3. It is possible to convert carbon suboxide monomer to malonic acid through reaction with water [53]. This would be an attractive alternative for malonic acid production because the carbon suboxide monomer can be created directly from carbon monoxide. Carbon suboxide monomer also reacts with ammonia and aniline to form malonamide and malonanilide, hydrogen chloride to form malonyl chloride and bromine to form dibromomalonyl bromide [53]. Carbon suboxide monomer can be used as a carbon source for the synthesis of nanotubes [54]. Experiments have been carried out which demonstrated that the monomer can be copolymerized with polyamide 6 [55] as well as polyethylene [56] to produce film grafts with interesting properties. The monomer is also very useful in various organic cycloaddition reactions which can be used to synthesize various benzimidazole and coumarin derivates which are an important class of heterocyclic compounds of pharmacological interest

[57, 58]. It has also been demonstrated that carbon suboxide reacts with a great variety of organometallic compounds allowing for the synthesis of unusual metal derivatives[59]. The polymer form of carbon suboxide has also been shown to produce glassy carbon [48] and amino acids [24, 26, 27]. Furthermore, ladder polymers similar to that of carbon suboxide polymer have been shown to have interesting optical, electrical, and magnetic properties [29]. There are several methods available for synthesizing carbon suboxide including dehydration of malonic acid with P_4O_{10} at 140-150^oC, thermolysis of 0,0,-diacetyltartaric anhydride in vacuo at 600-700^oC, pyrolysis of diethyl oxaloacetate in the presence of acetic anhydride at 850-880^oC, and dehalogenation of dibromomalonyl chloride with zinc [53]; the method of synthesizing carbon suboxide from a plasma discharge however has not been completely investigated.

The intimate role between carbon monoxide and carbon suboxide has been evident throughout the literature since the first published observation by Brodie. Carbon monoxide is essential, as is dicarbon monoxide, as precursors for the direct gas phase production of carbon suboxide. The route of carbon suboxide production discovered by Diels, from a global perspective, fundamentally relies on several chemical steps and makes for an interesting comparison; these steps are as follows: carbon suboxide is formed by the dehydrogenation of malonic acid, malonic acid is produced from chloroacetic acid, chloroacetic acid is produced by the chlorination of acetic acid, acetic acid is produced from methanol and carbon monoxide, and methanol is produced from carbon monoxide and hydrogen. Therefore the indirect pathway of carbon suboxide formation ultimately starts with synthesis gas and takes a chemical detour to arrive at carbon suboxide whereas the more direct route can convert carbon monoxide to carbon suboxide directly. When considering the industrial production of carbon suboxide the selected precursors can be chosen from any of the aforementioned stages and simply depends on the cost of the precursors as well as their availability. Therefore, with these factors in mind, the

production of carbon suboxide via plasma may be the best alternative for large scale production as synthesis gas is readily available and can be relatively inexpensive.

1.4 Introduction to Nonthermal Plasma-chemistry

1.4.1 Plasma Physics

Plasma is often considered to be the fourth state of matter. Beginning with a solid such as ice if one were to add energy to the ice it would soon melt and form a liquid. If more energy was added to the liquid it would soon become a gas. This is typically all that is taught in grade school however if you continue this process and add more energy to the gas it will become a plasma. A plasma is an ionized gas. There so much energy in the gas that the electrons are removed from their atoms and molecules. The most popular example of a plasma is the sun where energy is constantly being generated by thermonuclear fusion reactions resulting in a giant plasma ball. The sun is an example of a thermal plasma and is considered to be in equilibrium however it is also possible to have cold or non-equilibrium plasmas.

A thermal plasma can have gas temperatures on the order of 10,000 K and higher but it is also possible to create a plasma where the gas temperature is near room temperature, 300 K. This is accomplished by using electric fields to initiate and sustain the ionization process without heating of the gas molecules. In this way it is possible to directly add energy to the electrons in the gas. When a large enough electric field is present electrons can gain energy, cause ionization and therefore electron multiplication and generate excited species and radicals; as this process takes place energy transfers from the electric field to the electrons and finally to the gas molecules. On one hand if the current of electrons is not controlled the plasma will naturally begin to heat up; this is what happens for example with arcs used for welding. On the other hand if the current is controlled it is still possible to sustain ionization and radical formation processes

while maintaining a low gas temperature. This type of plasma is considered nonthermal plasma and is often characterized by its non-equilibrium nature. A thermal plasma is considered to be at equilibrium because there is a normal distribution of energy which means that the mean energy of the electrons is equal to the mean energy of the gas molecules, $T_e = T_{gas}$. For nonthermal plasmas the temperature of the electrons are typically much higher than the gas temperature as well as the vibrational and rotational temperatures (T_{gas}, T_{vib}, T_{rot}) < T_e. More accurately nonthermal plasmas typically have temperatures with the following distribution: ($T_{gas} = T_{rot}$) < ($T_{vib} = T_{elec}$) < T_e, where T_{elec} is the temperature of electronic excitation.

1.4.2 Catalysis and Plasma

A catalyst is able to increase the rate of reaction without affecting the equilibrium of the products and reactants; there are two main mechanisms that catalysts can use to do this. The important idea of catalysis, proposed by the great chemist Linus Pauling, suggests that a catalyst works by stabilizing the transition state of a reaction. Therefore an effective catalyst will bind tightly to the transition state of a reaction, but not to the reactants or products, resulting in an increase in the reaction rate. The mechanism explains one way to lower the activation barrier of a reaction. Alternatively ionic reactions and reactions with vibrationally excited molecules have an interesting effect on reactions. Ion reactions do not suffer for the columbic repulsion forces that are responsible for the activation barriers and therefore occur largely unimpeded; although this can appear to be very beneficial in speeding up reactions it is worth noting that ion production is a very energy intensive process. Reactions with vibrationally excited molecules also reduce energy barriers when compared to the ground state reaction; vibrational excitation requires much less energy than ion generation but still results in an excess energy requirement when compared to neutral and ground state reactions. Nonthermal plasma relies on both ion production and vibrational excitation reactions to do chemistry. The benefits that can be had

from nonthermal plasma are largely in the catalytic selectivity which can be quite controllable by adjusting parameters such as the reduced electric field (E/n). Although the plasma process may be energy intensive, the selective nature of the plasma can be quite useful.

Nonthermal plasma-chemistry therefore has many benefits that cannot be obtained using normal gas phase chemistry. Typical gas phase chemical reactions are driven by the use of heat, pressure and catalysts; all of these factors add to the cost for industrial chemical processing. Efficiencies for these processes can be very low due to heat losses; the low efficiencies means that a lot of energy is being wasted in the process and the process can be more expensive to run. High pressure processes tend to increase operating costs due to pumping, and increase capital costs due to increases in the thickness of reactor walls. Catalysts can help to speed up reactions and can help reduce reactor sizes and therefore capital costs for industrial processing; however catalysts are commonly easy to poison, can be difficult to work with and can be expensive. From an industrial perspective all of these considerations are taken into account when considering if a process can be economically viable, and many of them are, however there are many more processes that are not. For the latter case these chemical processes require an alternative solution in order to become economically viable.

Nonthermal plasma processing has many attractive features when compared to normal gas phase processing. By maintaining low temperatures in nonthermal plasma processing the heat losses experienced in high temperature gas phase processing can be minimized and therefore similar processes can be run at lower temperatures. Higher efficiencies and selectivity's can be possible because energy is going directly into electrons which then do chemical work; this can be much more efficient then heating up gas molecules to have them do chemical work. Many of these plasma processes can be run at atmospheric pressure and do not require additional

catalysts, although synergistic effects can be had between catalysts and plasma chemistry. The major cost for plasma processing can be the power supplies; however some good supplies can have efficiencies greater the 80%. Typically the major source of losses in efficiency is from losses in the conversion of electrical energy to heat. Nonthermal plasma chemistry can be very complex and difficult to describe accurately, the engineering can be difficult and sometimes materials can be expensive; however nonthermal plasmachemical processing offers many advantages as an alternative technology and may prove to be valuable.

1.4.3 The Dielectric Barrier Discharge

There are several methods of generating nonthermal plasmas but the main goal is to control of the plasma current. If the current is not controlled the plasma may achieve equilibrium conditions, assuming the power supply can support it, such as observed in hot plasmas like an arc. Typically the current can be limited using various tricks in the external circuit such as ballasting or pulsing. Dielectric barriers provide a method of limiting current by placing a dielectric material directly in the path of current flow. A simple explanation of the dielectric barrier discharge (DBD) will be provided here but a very good and detailed explanation can be found in literature [52].

When a high enough voltage is applied between two electrodes separated by some distance breakdown occurs. Typically this happens at about 3 kV/mm in atmospheric pressure air. When a dielectric material is placed between the electrodes, Figure 4, the dielectric strength of the gap is increased and DC current is largely impeded, however AC current can still flow. When an AC signal is applied to this new configuration a high electric field is generated in the gap and breakdown can still occur. When breakdown occurs the flow of current is now allowed to transfer to the electrode and charge simply accumulates on the surface of the dielectric material.

This process allows the discharge current to be controlled and generates a nonthermal 'cold' plasma with gas temperatures near room temperature.

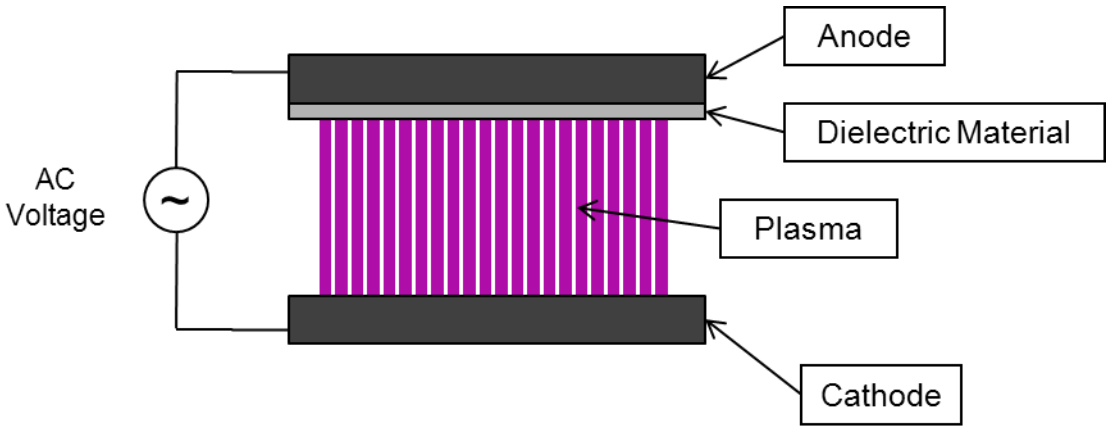

Figure 4 Schematic of Dielectric Barrier Discharge (DBD)

1.5 Thesis Objectives

The main objective of this thesis is to explore the chemistry that occurs between carbon and oxygen when carbon monoxide is stimulated to a nonthermal plasma state, a state that can uniquely provide insight of the vibrational excited chemistry at low gas temperatures. To fulfill the main objective several steps were taken and are described as follows.

Based on previous literature it has been shown that carbon suboxide is produced when carbon monoxide is excited either by radiolysis or nonthermal plasma and therefore a thermodynamic analysis of the molecule is necessary. Section 2 explores the thermodynamics of carbon suboxide including formation enthalpies and phase change data ; also considered are the equilibrium states of the several oxides of carbon. Within the plasma equilibrium is not an accurate assumption and therefore kinetic analysis is a vital tool. The kinetics of carbon

suboxide formation are considered in Section 2.3. Many experimental techniques were used to study the carbon monoxide plasma and these techniques along with reactor design and experimental setup are all described in Section 3. Experimental results from the techniques and setups describe in Section 3 are presented in Section 4. Some of the work presented here has been published and is partially included within Sections 2, 3, & 4 [12].

2. THERMODYNAMICS AND KINETICS OF CARBON SUBOXIDE*

2.1 Thermodynamic Properties

Thermodynamic analysis can provide a lot of valuable information regarding the properties and structure of molecules. In order to gain better insight into the carbon suboxide molecule its thermodynamic properties are evaluated. These properties can then be compared with the properties of other molecules to begin to understand how the might react chemically with one another. More accurate analysis of these chemical reactions can then be determined through the development of a kinetic model.

Determining the thermodynamic properties of carbon suboxide experimentally is a somewhat difficult task owing to its reactive nature. Although it is a stable molecule under room temperature and pressure conditions and can be stored in a sealed container without decomposition or polymerization, it is very sensitive to humidity. If care is not taken during the synthesis of the carbon suboxide monomer it will undergo polymerization and hydration reactions. Therefore while trying to obtain thermodynamic properties of the monomer partial polymerization and contamination of the product is a concern.

There exists however two main papers that have explored the thermodynamic properties of the substance and provide a basis for a more complete thermodynamic analysis [60, 61]. Thermodynamic information of carbon suboxide monomer gathered from these papers is presented in Table 1. The formation enthalpy for the gas phase monomer published by Kybett was -97.89 kJ/mol however this number was reviewed by Chase [62] and better estimation was determined to be -93.64 kJ/mol which was reinforced later by Simmie [63]. The carbon

* Part of the data reported in this chapter is reprinted with permission from Geiger, R., Staack, D., *Analysis of Solid Products Formed in Atmospheric Non-thermal Carbon Monoxide Plasma* Journal of Physics D: Applied Physics, 2011. **44**(27) by IOP Publishing Ltd

suboxide monomer resembles the other oxides of carbon, namely carbon monoxide and carbon dioxide, and it is interesting to compare formation enthalpies; carbon dioxide has the lowest formation enthalpy at about -393 kJ/mol, carbon monoxide is a little higher as about -110 kJ/mol and carbon suboxide is only slightly higher than carbon monoxide at about -94 kJ/mol. The natural phase of these three oxides of carbon under ambient conditions is that of a gas; however carbon suboxide boils at 6.7 C which is much higher than both carbon monoxide and carbon dioxide. This allows for an easy separation process to be developed for a mixture of these oxides of carbon.

Table 1 Thermodynamic properties of carbon suboxide monomer and polymerized carbon suboxide

Species	Properties	Value	Units	Reference
$C_3O_{2(g)}$	ΔH_f	-93.64	kJ/mol	[62, 63]
	ΔS^o	276.07	J/mol*K	[62]
	ΔG_f	-175.95	kJ/mol	
	C_p	67	J/mol*K	[62]
	ΔH_{vap}	23.66	kJ/mol	[60]
$C_3O_{2(l)}$	ΔH_f	-121.50	kJ/mol	[60]
$(C_3O_2)_n$	ΔH_f	-230.14	kJ/mol	[60]
	$\Delta H_{polymerization}$	-78.71	kJ/mol	[60]
Other	$\Delta H_{polymerization}$ *(gas to solid)*	-136.50	kJ/mol	[60]
Reference conditions are at standard temperature and pressure: T_{ref} = 25°C, P_{ref} = 1 bar and on a per mole of C_3O_2 basis.				

The review made by Chase used the Shomate equation format and extracted coefficients in order to determine the temperature dependence on the thermodynamic properties of carbon suboxide monomer. The Shomate equations are presented in equations 1.1 – 1.3 for the specific heat, enthalpy and entropy respectively. The variable *t* is equal to the temperature in Kelvin divided by 1000 (t = T/1000). The coefficients provided by Chase for carbon suboxide monomer are given in Table 2.

$$C_p{}^o = A + B * t + C * t^2 + D * t^3 + \frac{E}{t^2} \qquad \text{(Eq 1.1)}$$

$$H^o - H^o{}_{298.15} = A * t + \frac{B * t^2}{2} + \frac{C * t^3}{3} + D * \frac{t^4}{4} - \frac{E}{t} + F - H \qquad \text{(Eq 1.2)}$$

$$S^\circ = A * \ln(t) + B * t + \frac{C * t^2}{2} + \frac{D * t^3}{3} - \frac{E}{2 * t^2} + G \qquad \text{(Eq 1.3)}$$

Table 2 Shomate coefficients for carbon suboxide monomer

Temperature (K)	298-1200	1200-6000
A	51.83223	106.5761
B	82.07920	3.008431
C	-44.90311	-0.585714
D	9.130785	0.039383
E	-0.494976	-12.06958
F	-114.0219	-153.2486
G	313.4544	367.6627
H	-93.63792	-93.63792
Reference	[62]	[62]

The Shomate equations provide all the thermodynamic properties for carbon suboxide over a wide range of temperatures. For convenience these properties are plotted here; Figure 5 illustrates the entropy as a function of temperature, Figure 6 the enthalpy and Figure 7 the specific heat. The temperature range is from 298-6000 K, which covers most of the gaseous phase since carbon suboxide condenses at about 280 K. It is also worth noting that carbon suboxide easily reacts with itself to form a polymer and is more likely to do so at higher temperatures; for this reason and simply due to the reactive nature of the molecule the range of temperature provided here is largely theoretical and the molecule may not even exist, or are short-lived, at temperatures far from room temperature.

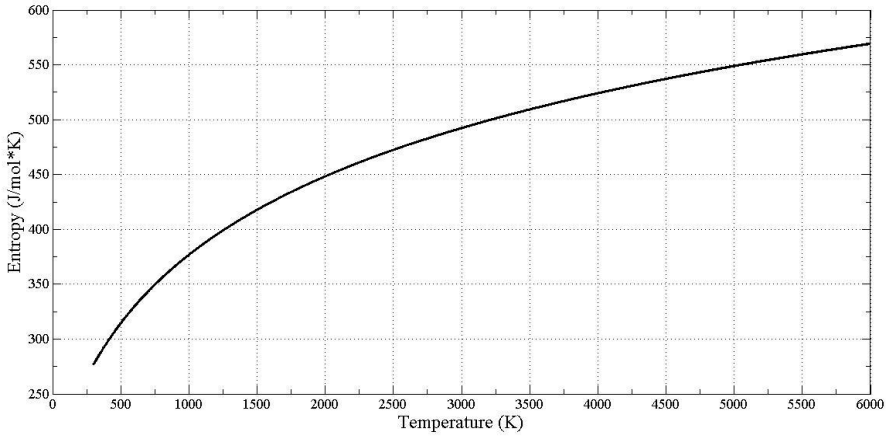

Figure 5 Entropy of carbon suboxide monomer in the gas phase verses temperature

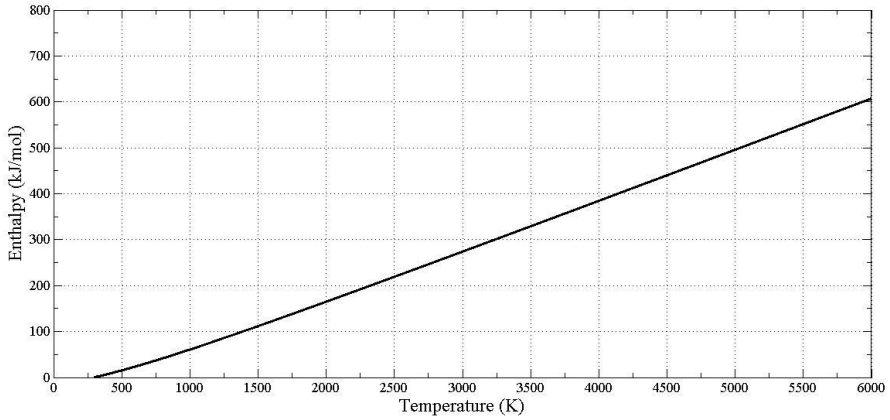

Figure 6 Enthalpy of carbon suboxide in the gas phase verses temperature

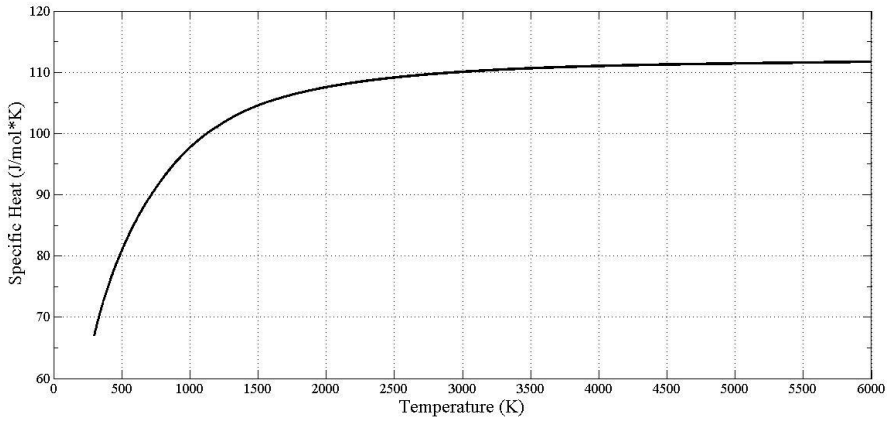

Figure 7 Specific heat of carbon suboxide in the gas phase verse temperature

With the information provided from the literature it is possible to generate a P-v diagram to analyze the phases of the carbon suboxide molecule. The method to be used is a modified BWR equation [64] which should provide reasonably accurate results. In order to determine phase change properties of carbon suboxide the critical properties must be determined. The accuracy of the critical properties is crucial due to the sensitivity of the modified BWR equation of state.

The method to be employed is the Joback method [65]. Although there are several methods that claim to provide better results [66] the Joback methods is the easiest and will provide a sufficient starting point for the analysis. The critical properties presented in Table 3 were determined using the Joback group method, the data provided in Table 4 and the experimental boiling temperature of carbon suboxide of T_b= 279.95 K. The critical temperature of carbon suboxide is 453.14 K and the critical pressure is 99.2 bar. These numbers were obtained using the boiling temperature of carbon suboxide at 279.95 K and plugging the group properties from Table 3 into equations 2.4, 2.5 and 2.6 respectively. The critical temperatures and pressures for the carbon dioxide and carbon monoxide gases are obtained from the Textbook for Fundamentals of Engineering Thermodynamics [67].

Table 3 Joback method results for carbon suboxide

Property	Joback Results
T_c (K):	453.13
P_c (bar):	99.20
V_c (cm3/mol):	197.5
ω:	0.3886
T_b(K):	279.95 [1, 68]
T_f(K):	161.85 [68]

$$T_c = T_{br}\left[0.584 + 0.965\sum G_i - \left(\sum G_i\right)^2\right]^{-1} \quad \text{(Eq 1.4)}$$

$$P_c = \left[0.113 + 0.0032 \cdot N_A - \sum G_i\right]^{-2} \quad \text{(Eq 1.5)}$$

$$V_c = 17.5 + \sum G_i \quad \text{(Eq 1.6)}$$

$$\omega = \frac{3}{7}\frac{T_{br}}{(1 - T_{br})} \quad \text{(Eq 1.7)}$$

Table 4 Joback groub contributions used for carbon suboxide

Group	Tc	Pc
=C=	0.0026	0.0028
=O (other)	0.0143	0.0101

The compressibility factor (Z) is expressed in terms of compressibility of a simple fluid and a reference fluid determined using the relation given in the paper by Pitzer [64]:

$$Z = Z^{(0)} + \omega Z^{(1)} \quad \text{(Eq 1.8)}$$

$$Z^{(1)} = \frac{\omega}{\omega^{(r)}}(Z^{(r)} - Z^{(0)}) \quad \text{(Eq 1.9)}$$

The compressibility factors are calculated using a polynomial equation, Eq 2.10-2.13, with reduced volume (V_r) as the variable, derived by Benedict et al [69]. The BWR equation is used for the simple and the reference fluid properties. Relationship between vapor saturation pressure, boiling point temperature and acentric factor are defined to evaluate the compressibility factors, given in Eq 2.14 and 2.15.

$$Z = \frac{P_r V_r}{T_r} = 1 + \frac{B}{V_r} + \frac{C}{V_r^2} + \frac{D}{V_r^5} + \frac{c_4}{T_r^3 V_r^2}(\beta + \frac{\gamma}{V_r^2})e^{-\frac{\gamma}{V_r^2}} \quad \text{(Eq 1.10)}$$

$$B = b_1 + \frac{b_2}{T_r} + \frac{b_3}{T_r^2} + \frac{b_4}{T_r^3} \quad \text{(Eq 1.11)}$$

$$C = c_1 - \frac{c_2}{T_r} + \frac{c_3}{T_r^3} \quad \text{(Eq 1.12)}$$

$$D = d_1 + \frac{d_2}{T_r} \quad \text{(Eq 1.13)}$$

$$\omega = -\log(P_r^s) - 1 \qquad @\ T_r = 0.7 \quad \text{(Eq 1.14)}$$

$$\ln(P_r^s) = 5.92714 - \frac{6.09648}{T_r} - 1.28862.\ln(T_r) + 0.169347.T_r^6 + \omega(15.2518 - \frac{15.6875}{T_r} - 13.4721.\ln(T_r) + 0.43577.T_r^6) \quad \text{(Eq 1.15)}$$

$$[\ @\ T_r = 0.7\ ]$$

The values of all the constants are different for the simple compound and the reference compound. Isotherms for different values of T_r are generated on the P_r versus V_r graph using the correlation in equation Eq 2.10. By substituting the values for boiling point reduced temperature (T_{br}) in equation 2.7 the acentric factor is obtained. Lee and Kessler extended this approach in their research to develop analytical correlations for enthalpy departures (Zh) given in Eq 2.16 and Eq 2.17.

$$Zh = Zh^{(0)} + \omega Zh^{(1)} \quad \text{(Eq 1.16)}$$

$$Zh^{(1)} = (Zh^{(r)} - Zh^{(0)}) \quad \text{(Eq 1.17)}$$

The P-V-T properties over a range of temperatures and pressures along the saturation curve are obtained using the analytical correlations for all the constituent gases/compounds. The value of acentric factor for reference compounds is $\omega^{(r)} = 0.3978$. If a mixture of carbon suboxide and other gases are to be evaluated, say for instance is the carbon suboxide was produced from synthesis gas and therefore contains other products, the pseudo-critical properties of mixtures cannot be obtained using Kay's additive rule have significant errors instead a modified set of

formula for mixture property calculations is used for improved accuracy; these formulas are given in Eq 2.18 - 2.23.

$$V_{ci} = \frac{Z_{ci}.R.T_{ci}}{P_{ci}} \quad \text{(Eq 1.18)}$$

$$Z_{ci} = 0.2905 - 0.085.\omega_i \quad \text{(Eq 1.19)}$$

$$V_c = \frac{1}{8}\sum_j \sum_k y_j y_k \left(V_{cj}^{1/3} + V_{ck}^{1/3}\right)^3 \quad \text{(Eq 1.20)}$$

$$T_c = \frac{1}{8V_c}\sum_j \sum_k y_j y_k \left(V_{cj}^{1/3} + V_{ck}^{1/3}\right)^3 \sqrt{T_{cj}T_{ck}}. \quad \text{(Eq 1.21)}$$

$$\omega = \sum_j y_j \omega_j \quad \text{(Eq 1.22)}$$

$$P_c = \frac{Z_c.R.T_c}{V_c} = \frac{(0.2905 - 0.085.\omega).R.T_c}{V_c} \quad \text{(Eq 1.23)}$$

The heat of vaporization is simply the difference between the enthalpies at saturated vapor and saturated liquid states and is a function of temperature. In order to determine the vaporization enthalpy of carbon suboxide as a function of temperature the Clausius-Clapeyron equation Eq 2.24 is employed.

$$\ln\frac{P_1}{P_2} = \frac{\Delta h}{R}\left(\frac{1}{T_2} - \frac{1}{T_1}\right) \quad \text{(Eq 1.24)}$$

Based off of the calculated critical properties of carbon suboxide and utilizing the well-known concept of corresponding states it is a simple matter to convert to reduced properties. The reduced properties are then plugged into the modified BWR equation and the P-v-T data can be extracted. In order to evaluate this data over wide ranges a Matlab program was created and

used to generate the P-v diagram in Figure 8 which shows various isotherms and the P-T diagram in Figure 9.

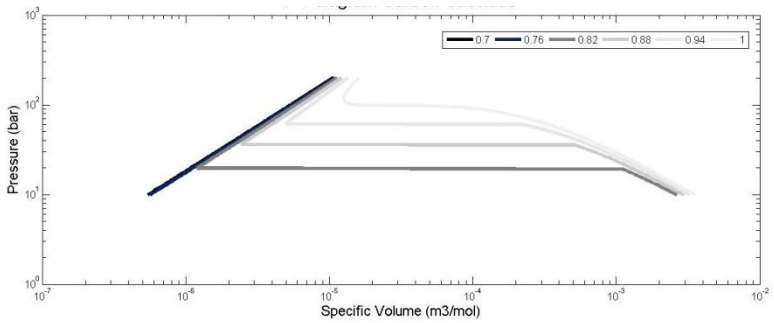

Figure 8 P-v diagram of carbon suboxide

The P-v diagram for carbon suboxide monomer is very near ambient conditions and is therefore quite far from other oxides of carbon, namely carbon dioxide and carbon monoxide, which has several implications. When considering the mixture properties of a gas it is often important to consider enthalpy and entropy departures, however these departures will most likely be negligible. To reinforce this assumption estimates were made for these enthalpy departures and errors less than 0.01% were determined. Therefore an ideal gas mixture assumption is quite valid and can be assumed for this type of mixture calculation.

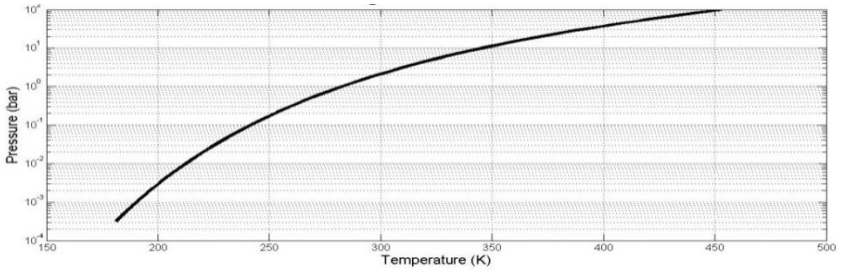

Figure 9 P-T diagram for carbon suboxide

The enthalpy of vaporization as a function of temperature was also determined. These values are derived using Eq 2.24 and are plotted in Figure 10.

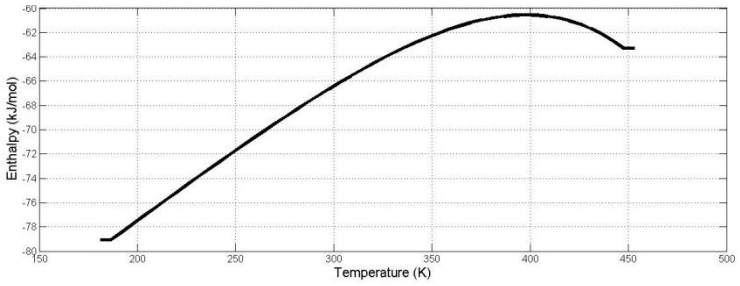

Figure 10 Enthalpy of vaporization of carbon suboxide as a function of temperature

2.2 Equilibrium States of Oxides of Carbon

The equilibrium thermodynamics of carbon monoxide demonstrates how carbon monoxide is actually a meta-stable molecule under standard conditions. The well-known Bourdouard reaction shown in Table 5 equation A below is commonly used to explain the disproportionation of carbon monoxide into carbon dioxide and solid carbon. At equilibrium this reaction shows

that carbon monoxide is most stable at temperatures above 1200 K while below these temperatures carbon dioxide and solid carbon become more favorable.

Table 5 Equations considered for the thermodynamic equilibrium calculations

	Independent Stoichiometric Equations
(A)	$2CO \Leftrightarrow C_{(s)} + CO_2$
(B.1)	$4CO \Leftrightarrow C_3O_2 + CO_2$
(B.2)	$n(C_3O_2) \Leftrightarrow (C_3O_2)_n$
(B.3)	$C_3O_2 \Leftrightarrow 2CO + C_{(s)}$

If carbon monoxide, carbon dioxide, solid carbon, carbon suboxide monomer and carbon suboxide solid polymer are all considered to be in equilibrium, that is the Gibbs free energy of equations B.1, B.2 and B.3 in Table 5 is minimized, the composition is plotted in Figure 11(a). It can be seen that the equilibrium consists of about 50% carbon dioxide and 50% solid carbon on a mole basis at 300K and 1 atm. As the equilibrium temperature is increased the composition will begin to favor carbon monoxide as can be seen in Figure 11(a), this dependency is the same as the equilibrium predicted by the Bourdouard equation. Considered species in this general thermodynamic calculation shown in Figure 11(a) are gases: C, C_2, CO, CO_2, C_2O, C_3O_2, O, O_2, O_3, and solids: carbon suboxide polymer, $C_3O_{2(n)}$, and graphite, $C_{(gr)}$.

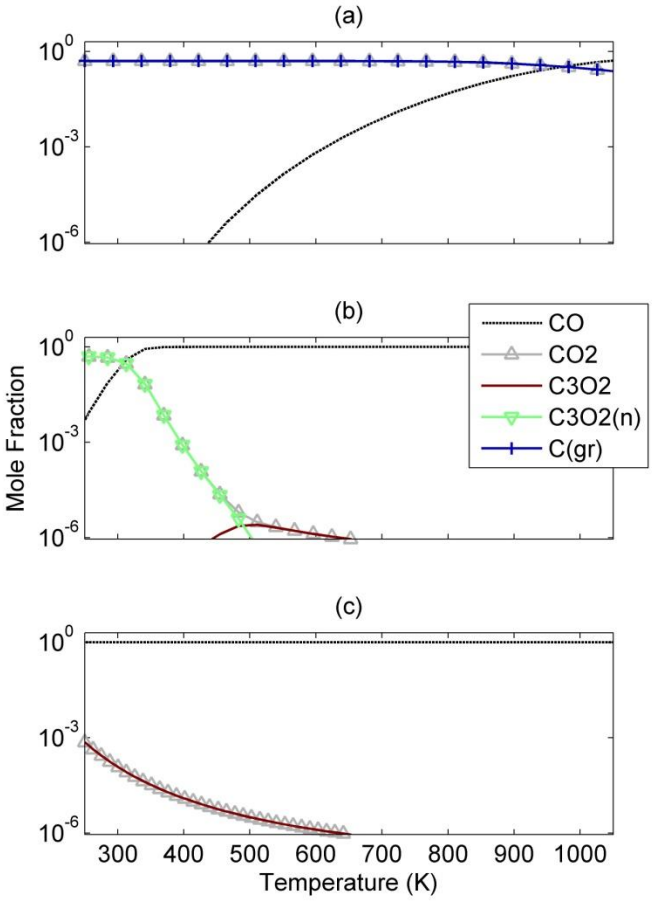

Figure 11 Thermodynamic equilibrium calculations for various temperatures considering only the following:

a) Equations B.1, B.2, B.3 b) Equations B.1 and B.2 c) Equation B.1

Only the five highest concentration species are plotted. Thermodynamic information for carbon suboxide monomer and polymer was taken from the papers of McDougall and Kybett [60, 61] while other species data is taken from the GRI mechanism [70] and used Cantera [71] with Matlab for the equilibrium calculations shown here. From these simulations it can be understood that carbon monoxide is not thermodynamically favored under ambient conditions; equilibrium is a graphite and CO2 mixture. The fact that CO exist at ambient conditions is

simply due to kinetic limitations. Only at temperature above 973K is CO thermodynamically favored.

To further investigate the relative stability of these molecules and the possible effects of the plasma discharge on carbon monoxide a comparison can be made to the situation when $C_{(s)}$ is removed from the equilibrium calculations. The removal of $C_{(s)}$ from the equilibrium calculations is of course no longer the actual equilibrium state as in reality $C_{(s)}$ is a possible product; however, this pseudo-equilibrium is a useful tool to analyze the driving forces which may be important in the plasma and other kinetic effects. In this situation it is assumed that reactions which lead to C_3O_2 formation are kinetically faster in such a way that $C_{(s)}$ is kinetically inaccessible by comparison. The precise mechanism (including the neutral kinetics, various intermediate plasma species stimulating reactions or even other catalysts) of the kinetics which leads to the removal of $C_{(s)}$ in this pseudo-equilibrium is irrelevant due to the generalities of the equilibrium calculation. When solid carbon is removed from the equilibrium calculation the result is a new equilibrium composition, shown in Figure 11(b), consisting of about 50% carbon suboxide polymer and 50% carbon dioxide near ambient conditions. This equilibrium calculation can be considered as using only equations B.1 and B.2 of Table 5 as the independent stoichiometric equations.

In this consideration solid carbon suboxide polymers are favored over carbon monoxide at low temperatures. At only slightly higher temperatures, above 310 K, CO is favored and the polymer is relatively unstable. The thermodynamic analysis in Figure 11(b) obviously ignores the formation of known species, $C_{(s)}$, however it may be justifiable if the kinetics of $C_3O_{2(n)}$ formation are significantly faster than the kinetics of $C_{(s)}$ formation (considered in more detail later). One further calculation can be made by removing the solid carbon suboxide polymer

from the calculation; this essentially results in only the single stoichiometric equation, B.1 in Table 5. Under these conditions carbon monoxide is the favored molecule however it is interesting to note that carbon suboxide monomer is tending to favor colder temperatures. At 300K carbon suboxide monomer and carbon dioxide are slightly more than 100 ppm of the composition. These thermodynamic simulations provide key information regarding the stability of carbon suboxide and carbon suboxide polymer relative to the carbon monoxide molecule. Carbon suboxide is actually a favored product at and below temperatures of 300K if solid carbon is not considered in the calculation. Although carbon monoxide is in practice known to be stable under standard conditions it is actually a meta-stable molecule and its conversion to carbon suboxide, solid carbon, and carbon dioxide is kinetically limited at standard conditions. The room temperature kinetic limitation is due to the low probability of molecules with sufficient energy to overcome activation barriers when considering an equilibrium energy distribution function. The kinetic barrier can be overcome by the plasma discharge. In low temperature non-equilibrium plasmas differences between the vibrational and the translational and rotational energy distribution function is common. Typically T_{vib} (an approximation of the vibrational energy distribution function) is on the order of several thousand Kelvin while T_{gas} (representing the nearly equal rotational and translational energy distribution functions) is near ambient temperature. In plasmas this condition of $T_{vib} >> T_{gas}$ is due to electron impact excitation of the molecules and can accelerate the rate of reactions for meta-stable molecules towards chemical equilibrium at low gas temperatures; this is an example of what was referred to as selective catalysis in section 1.4.2.

2.3 Kinetics of Carbon Suboxide Formation from Carbon Monoxide

Proposed kinetic mechanisms for the production of carbon suboxide may include reactions 1-4 given in Table 6 as suggested by McTaggart [50]. The formation of carbon suboxide is

initiated by the reaction between ground state CO and an excited CO* molecule (excitation denoted with the asterisk) and is considered here to be the limiting reaction. In a plasma the CO* formation and rate of reaction (1) is greatly enhanced as it is formed through vibrational excitation of CO through collisions with electrons, CO + e → CO* + e. The model of C_3O_2 formation initiated by CO* rather than electron impact dissociation or ion reactions is based upon several reports describing various kinetics of carbon suboxide formation and will be considered shortly [50, 72-74]. It is thought that under atmospheric conditions ionic reactions do not play a significant role and the initiation step is through electron-collision excitation processes and not by negative or positive ion channels; these conclusions are summarized and explained in detail in the paper of Maksimov et. al [75]. Subsequent to reaction (1) which forms the necessary free carbon atom, C, an intermediate radical C2O is formed by reaction with CO. C3O2 gaseous monomer is formed by reaction of C2O with CO again. The monomer may react with itself at a surface to form the suboxide polymer. An alternative competing route is for the carbon atoms to form solid carbon reactions (5-6). Only the first reaction is listed as it is known that such nucleation reactions are typically limited by the initial reactions [76]. From an equilibrium stability perspective as shown earlier carbon solid formation is favored over carbon suboxide formation. However, taking as given the stimulation of reaction (1) by plasma, a simple comparison of reaction rates can determine whether the formed carbon atoms more readily follow a pathway leading to solid carbon or solid carbon suboxide formation. Known reverse reactions, leading to back to CO, or other plasma reactions farther down the reaction path, not detailed here, will affect this analysis and overall kinetics. The goal of this simple analysis is simply to initially determine to rough approximation whether solid carbon or solid carbon suboxide polymer may occur faster and under what conditions carbon suboxide formation may be favored.

Table 6 Reaction and standard pressure and temperature reaction rates leading to solid carbon and carbon suboxide formation from carbon monoxide

	Reaction			Rate		Ref.
(1)	$CO + CO^*$	→	$C + CO_2$			
(2)	$C + CO + m$	→	$C_2O + m$	6.3×10^{-32}	$[cm^6/molecule^2*s]$	[77]
(3)	$C_2O + CO$	→	C_3O_2	4.33×10^{-15}	$[cm^3/molecule*s]$	[78]
(4)	$n(C_3O_2)$	→	$(C_3O_2)_n$	6.6×10^{-14}	$[cm^3/molecule*s]$	[79, 80]
(5)	$C + C$	→	C_2	2.16×10^{-11}	$[cm^3/molecule*s]$	[76]
(6)	C_2	→	$C_{(s)}$			

Assuming a small amount of excited carbon monoxide reacts with carbon monoxide to form a small concentration of carbon the rate of formation of carbon suboxide can be compared to the rate of formation of solid carbon. This can be modeled as a function of initial carbon concentration by comparing the reaction rates of the initial reaction in pathway (2-4) to the initial reaction in pathway (5-6); the results of this calculation reaction (2) compared to reaction (5) (R2/R5) are shown in Figure 12. It can be seen that carbon suboxide should always tend to form faster (R2/R5>1) and that the suboxide formation is favored particularly at lower concentrations of atomic carbon. Both the thermodynamic and kinetic analysis suggests that carbon suboxide is the favorable product in comparison to CO and C(s) when small concentrations of excited carbon monoxide exist. Furthermore, it becomes clear that increasing the vibrational temperature of carbon monoxide while maintaining low gas temperatures should promote the production of carbon suboxide. Excessively high gas temperatures, however, may favor CO formation (from equilibrium calculations, Figure 11) and C(s) formation by comparison of reactions 2 and 5 as a function of temperature (Figure 13). These thermodynamic considerations suggest that highly non-equlibrium, low power density discharges such as corona and DBDs which generate CO* at low temperature may be more suitable for carbon suboxide formation rather than higher power density and higher temperature (though still non-equilibrium) glow discharges and gliding arc discharges.

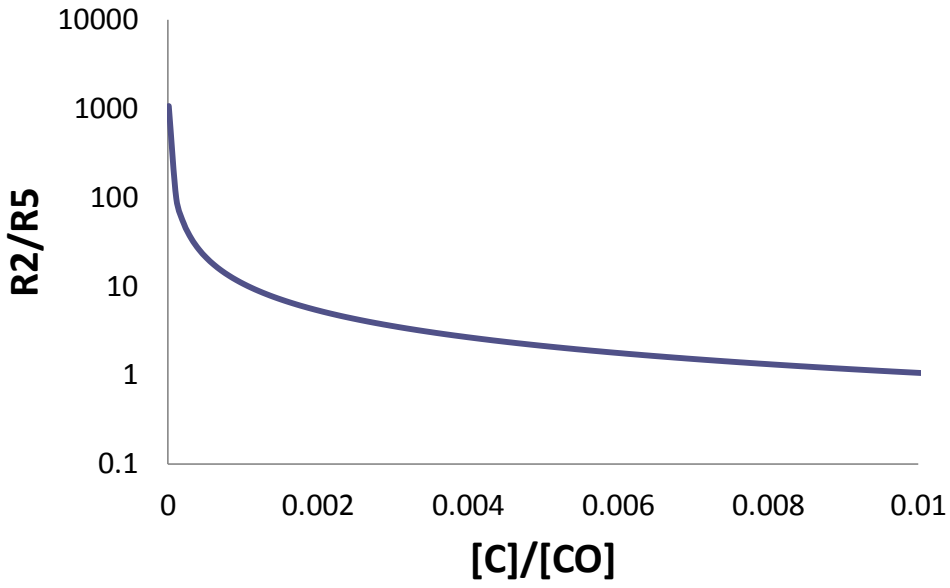

Figure 12 The rate of formation of solid carbon suboxide polymer relative to the rate of formation of solid carbon if plotted verse initial gaseous carbon concentration relative to the initial carbon monoxide concentration at a constant temperature of 300K

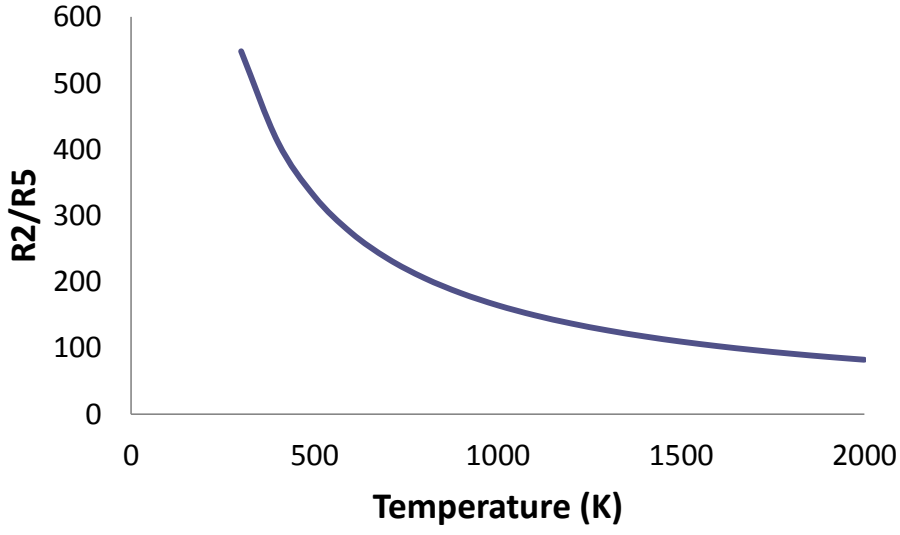

Figure 13 Relative reaction rates for formation of carbon suboxide relative to solid carbon as a function of temperature at [C]/[CO] = 3. 10E-04

From the kinetic analysis thus far it is quite apparent that carbon suboxide production may depend strongly on the production and subsequent reactions of atomic carbon. Atomic carbon is very reactive and has a lot of free energy; it can be quite difficult to measure reaction rates near ambient conditions [77]. As mentioned previously the initial production of carbon in nonthermal carbon monoxide plasma can occur through direct electron impact dissociation of carbon monoxide or through reactions of excited carbon monoxide. In the previous analysis it was unimportant which mechanism produced the carbon however a more detailed kinetic analysis requires a more specific account of these two possibilities.

Brown and Bell analyzed the kinetics of carbon monoxide oxidation in a radiofrequency carbon dioxide electric discharge and required rate coefficients for electron impact dissociation of carbon monoxide [81]; however cross section information was not available for such low electron energies therefore they used a crude comparative method to derive the reaction rate coefficient which they determined. The reaction $e^- + CO \rightarrow C + O + e^-$ was compare to the dissociation of oxygen by electron impact, $e^- + O_2 \rightarrow O + O + e^-$ because the cross section data for the latter reaction was available therefore the rate constant can be calculated directly using Eq 2.25 which assumes a Maxwellian distribution. Brown and Bell assumed the relation shown in Eq 2.26 between the rate coefficients for oxygen dissociation relative to carbon monoxide dissociation in order to predict the carbon monoxide dissociation rate coefficient, k_2. The results are shown in Figure 14.

$$k_1 = \sqrt{\frac{8}{\pi m_e}} (kT_e)^{-3/2} \int_0^\infty \varepsilon \sigma_1(\varepsilon) e^{-\varepsilon/kT_e} \, d\varepsilon \qquad \text{(Eq 1.25)}$$

$$\frac{k_2}{k_1} = \frac{\varepsilon_2 + kT_e}{\varepsilon_1 + kT_e} e^{\frac{\varepsilon_1 - \varepsilon_2}{kT_e}} \qquad \text{(Eq 1.26)}$$

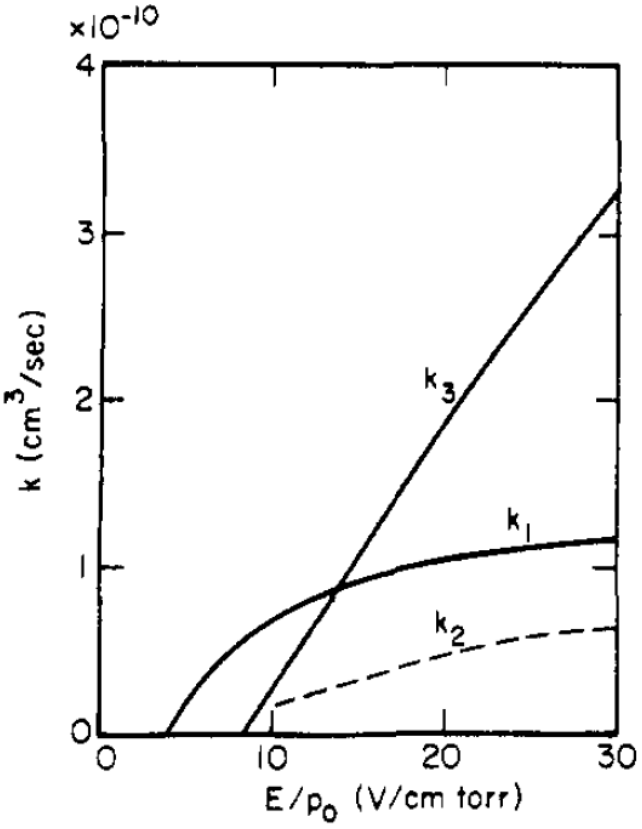

Figure 14 Rate coefficients for the electron impact dissociation of O_2 (k_1), CO (k_2), and CO_2 (k_3) [81]

It can be estimated by the work of Brown and Bell that the predicted dissociation rates around Te = 2 eV relatively slow, k ~ 7.4e-12 cm^3/s [82]. Perhaps a better approximation can be had by extrapolating from more recent cross section data provided by Cosby [83]. By extrapolating the cross section data provided by Cosby and solving Eq 2.25 the reaction coefficient at Te = 2eV is k = 1.66e-11 cm^3/s and at Te = 1eV the value of k is 1.94e-14 as shown in Figure 15.

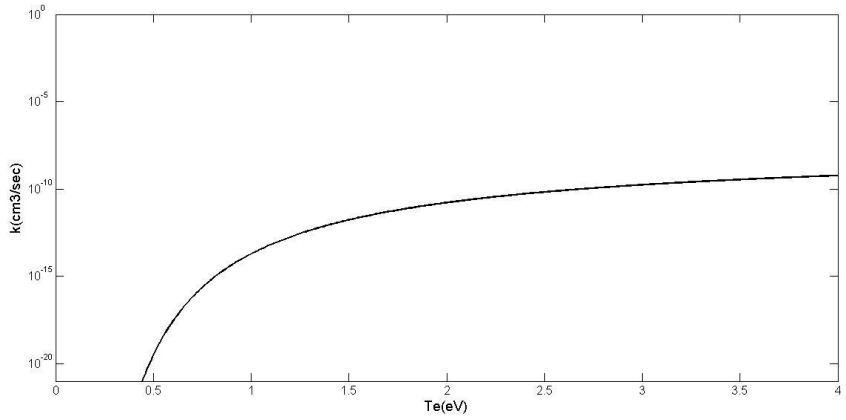

Figure 15 Reaction coefficients for the dissociation of carbon monoxide by electron impact extrapolated from the data provided by Cosby [83]

Since the electron temperature for typical nonthermal plasmas are typically around 1 eV it is now possible to compare the reaction rate of electron impact dissociation to the reaction rate expected from dissociation due to excited carbon monoxide at Te =1eV. Estimates for the reaction $CO(a^3\Pi) + CO \rightarrow CO_2 + C$ are on the order of 1.4e-12 cm^2/s [84]; if this value is considered a valid approximation for the production of atomic carbon through vibrationally excited carbon monoxide than this reaction is about 100 times faster than electron impact dissociation. If the electron temperature increases beyond 1 eV however electron impact dissociation can begin to play a more important role in the mechanism of carbon suboxide formation. At the same time however the addition of carbon suboxide as a product can have a strong influence on the vibrational distribution of carbon monoxide by increasing the rate of vibrational relaxation due to collisions of excited CO and C_3O_2 [84]. This effect may eventually limit the production of carbon suboxide as its concentration increases.

There have been numerous studies on the flash photolysis of carbon suboxide which can be very helpful in understanding the kinetics of nonthermal carbon monoxide plasma [77, 85, 86].

During photolysis of carbon suboxide there are several possible radicals that can be produced including C, C_2, C_3, CO, C_2O, C_3O, O and polymerization can also be induced. Within the literature a wide range of incident wavelengths have been studies and the addition of various gases during photolysis has been utilized in order to understand the possible radicals that have been produced. In the paper of Morrow and McGrath the radical C_3 was observed while C_2 was very weakly observed while photolysis was carried out in the range of 230-290 nm [85]. This result led to the assumption that C_3 was being produced not from carbon building up, that is from C_2, rather it must be produced from the reaction of other radicals. It was also observed that the addition of oxygen suppressed the C_3 signal while concurrently reducing polymerization. They concluded that the C_2O radical can react with C_3O_2 through a quick multistep reaction to produce C_3 and CO. It was also suggested that the oxygen reacted with intermediates during the quick multistep reaction between C_2O and C_3O_2 therefore suppressing the C_3 signal. These results suggest that as the concentration of C_3O_2 produced in a carbon monoxide plasma increases it should be expected that C_3 may be produced and can lead to more soot production than polymer production; at the same time it is expected that large concentrations of oxygen may suppress polymerization reactions. Other possible routes for the production of C_3 may include reactions of C and C_3O_2 or C and C_2.

The wavelengths used by Morrow and McGrath are able to produce C_2O in an excited triplet and singlet state while longer wavelengths, greater than 290 nm, C_2O is produced in its ground state and in general for wavelengths above 200nm it is not possible to directly carry out the reaction $C_3O_2 \rightarrow C+2CO$ [86]. For the case of higher energy light, less than 200 nm, the direct production of primarily carbon and carbon monoxide from carbon suboxide becomes possible while avoid the formation of C_2O; it was also noted that if carbon monoxide is added to the carbon suboxide during photolysis in this vacuum ultra-violet region C_2O is produced [86]. This

important finding provides a method of producing atomic carbon atoms in the gas phase at ambient conditions which can be used to analyze the reactivity of carbon with various molecules. From the same paper of Braun et al. we are also provided with the perhaps the most important reaction when considering carbon suboxide production in a carbon monoxide plasma; this reaction is the reaction of C with CO to produce the C_2O radical. As mentioned in the previous initial kinetic analysis the production of carbon in the carbon monoxide plasma is assume to occur through reactions of excited carbon monoxide however they can also occur through the more energy intensive pathway of electron impact dissociation of carbon monoxide. In either case once the atomic carbon is produced it can react with carbon monoxide to produce the C_2O radical required for carbon suboxide production. This reaction is strongly dependent on pressure, occurs rapidly and at high pressures C_2O can be stabilized [86].

Once atomic carbon and dicarbon monoxide (C_2O) are available other reaction pathways become available. Using the mechanism shown in Table 7, reaction (1) produces carbon dioxide, while it is further possible that the reverse of this reaction can occur however this reaction has been demonstrated to be quite slow, $< 10^{-15} cm^3/s$ [87]. Another possibility is that atomic carbon can react with carbon monoxide as $C + C_2O \rightarrow C_2 + CO_2$. It has been suggested that at high pressures of carbon monoxide, within a microwave discharge, this reaction actually may have a greater contribution to the production of C_2 than reaction (6) [87]. Therefore without this reaction should be incorporated in order to develop an accurate mechanism; however this rate has not been measured. To make a rough approximate the reaction it will be considered that this reaction occur at the same rate as reaction (6) and it should be realized that the destruction of dicarbon monoxide and the production of carbon dioxide and carbon dimer are most likely being underestimated. Furthermore it may be possible that the conditions exist where reaction (7) becomes large enough as to inhibit the production of C_2O and therefore C_3O_2.

Table 7 Mechanism of carbon suboxide formation in nonthermal plasma with Te = 1 eV

	Reaction			A	n	Ea (J)	Ref.
(1)	$CO + CO^*$	→	$C + CO_2$	1.4e-12	0	0	[84]
(2)	$CO + e^-$	→	$C + O + e^-$	1.94e-14	0	0	[83]
(3)	$C + CO + m$	→	$C_2O + m$	6.3e-32	0	0	[77]
(4)	$C_2O + CO$	→	C_3O_2	4.33e-15	0	0	[78]
(5)	$n(C_3O_2)$	→	$(C_3O_2)_n$	6.6e-14	0	0	[79, 80]
(6)	$C + C$	→	C_2	2.16e-11	0	0	[76]
(7)	$C + C_2O$	→	$C_2 + CO_2$	2.16e-11	0	0	*See text*
(8)	$C + CO_2$	→	$CO + CO$	< 1e-15	0	0	[87]
(9)	$C + O_2$	→	$O + CO$	5.10e-11	-0.3	0	[88]
(10)	$C_2 + O_2$	→	$CO + CO$	1.10e-11	0	3168	[89]
(11)	$O + CO + m$	→	$CO_2 + m$	1.70e-33	0	1.26e4	[90]
(12)	$O + C_2O$	→	$CO + CO$	8.60e-11	0	0	[91]
(13)	$O + CO_2$	→	$CO + O_2$	2.81e-11	0	2.20e5	[90]
(14)	$O + O_2 + m$	→	$O_3 + m$	6.01e-34	-2.30	0	[92]
(15)	$O + O_3$	→	$O_2 + O_2$	8.00e-12	0	1.71e4	[93]
(16)	$CO + O_2$	→	$O + CO_2$	4.20e-12	0	2.00e5	[90]
(17)	$CO + O_3$	→	$O_2 + CO_2$	< 4.0e-25	0	0	[94]
(18)	$O_2 + O_2$	→	$O + O_3$	1.11e-11	0	4.15e5	[95]
(19)	$C_3O_2 + O$	→	$CO_2 + C_2O$	4.10e-14	0	0	[96]

3. EXPERIMENTAL DESIGN*

3.1 Carbon Monoxide Safety

These experiments were conducted using a tank a high purity carbon monoxide; whenever working with such high purities of carbon monoxide care must be taken. Carbon monoxide is a deadly, colorless, poisonous gas and can therefore be undetectable to the human senses. If too much carbon monoxide is consumed symptoms as low levels, around 150 ppm, may include headaches, fatigue, shortness of breath, nausea, dizziness. At higher levels symptoms can include mental confusion, vomiting, loss of muscular coordination, loss of consciousness, and ultimately death.

There are several precautions that can be taken while working with this gas which were implanted in this research. The first precaution is to have a carbon monoxide detector nearby that can alert you if concentrations in the room are getting too high. The room should have proper ventilation to ensure that any carbon monoxide the might have leaked will be ventilated. Finally a purge line can be arranged so that all of the working lines used for flowing carbon monoxide can be purged with some inert gas, in our case we simply used nitrogen. This purge ensures that no carbon monoxide remains in the lines and in the reactor after experiments have been conducted. If the lines are reactor are not purged the carbon monoxide will eventually leak into the room or could leak out if the system is disassembled. It is highly recommended that a procedure be developed whereby after running experiments the purging processes is always executed.

* Part of the data reported in this chapter is reprinted with permission from Geiger, R., Staack, D., *Analysis of Solid Products Formed in Atmospheric Non-thermal Carbon Monoxide Plasma* Journal of Physics D: Applied Physics, 2011. **44**(27) by IOP Publishing Ltd

3.2 General Setup

Several experimental setups were considered and tried however the basic setup requires only a few components which will be described in detail here. The choice of using nonthermal plasma reactor type was the dielectric barrier which was chosen out of convenience, as it provides a surface for the polymer to form which allows for easier sample collection and analysis; however other systems can theoretically be developed as well such as a corona system.

The experimental setup for producing carbon suboxide is illustrated in Figure 16. An Alicat Scientific digital flowmeter was used to feed ultra pure 99. 999% carbon monoxide to the reactor. The exhaust gas was measured using a SRI 8610C Gas Chromatograph (GC) equipped with a Helium Ionization Detector (HID) and a Thermal Conductivity Detector (TCD). The exhaust gas samples were taken using a syringe. The capability of the GC-HID/TCD instrumentation allowed for detection of gas concentrations in the range from the tens of PPM level up to one hundred percent. The temperature of the reactor can change with discharge power; in order to address temperature dependent kinetic issues for the system thermocouples were placed at the inlet and the exhaust in order to measure temperature.

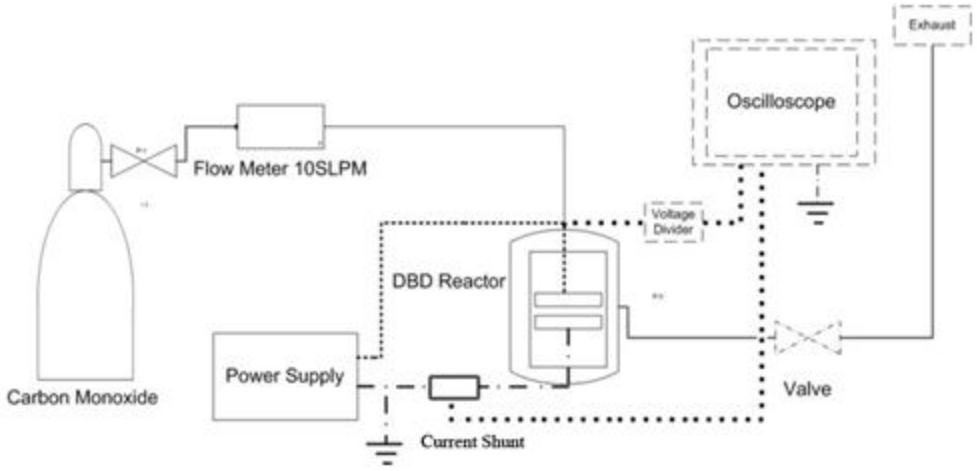

Figure 16 Schematic of Experimental Setup indicating gas and electrical flows

To generate the dielectric barrier discharge (DBD) plasma inside the reactor a variable power 200 watt ac power supply was used. Frequency could be controlled within the range of 25-30 kHz. Current voltage characteristics were measured using a voltage divider to measure the high voltage and measuring the voltage drop across a shunt resistor on the grounding line. These signals were read using a Lecroy WaveRunner 204MXi oscilloscope. From this data the product of current and voltage were averaged over several periods to give power measurements. This method provides similar results to Lissajous plot methods.

A SPEX 100m spectrophotometer was used to measure the spectrum of the carbon monoxide plasma emission. The light enters the spectrophotometer through a 100 μm slit and travels a focal length of 1m to a collimating mirror. The grating used has 2400 groves/mm which allowed for a precision of about 0.5 nm. The light is detected using a high speed 4 Picos digital ICCD.

3.3 Reactor Design

A planar dielectric barrier discharge reactor, Figure 17, was used for this study. The reactor was constructed from sections of two thick walled PVC tubes with aluminum rods 25 mm in

diameter running through them acting as electrodes. To the flush surface at the end of each tube, quartz discs, acting as the dielectric, being 1. 6 mm thick and 50 cm in diameter, were glued using silicone based glue. In later modification of the reactor one of the electrodes was modified so that the quartz disk was removable and held on with a vacuum chuck (rather than glued) – this facilitated weighting and analysis of the deposited films. Each of these PVC electrode configurations slid into an acrylic tube such that the quartz discs faced each other. O-rings provided a seal from the PVC to the acrylic and the distance between the quartz discs, approximately 2 mm, was set by the length of the acrylic tube. Two additional holes were made in one of the PVC tubes, lying just outside the quartz disc, which allowed for gas flow in and out of the otherwise airtight chamber. Excessive heating of the electrodes was mitigated by heatsinks attached to the electrodes. This setup provided a controlled environment and large plasma volume to reactor volume ratio in order to better study the plasma chemistry taking place.

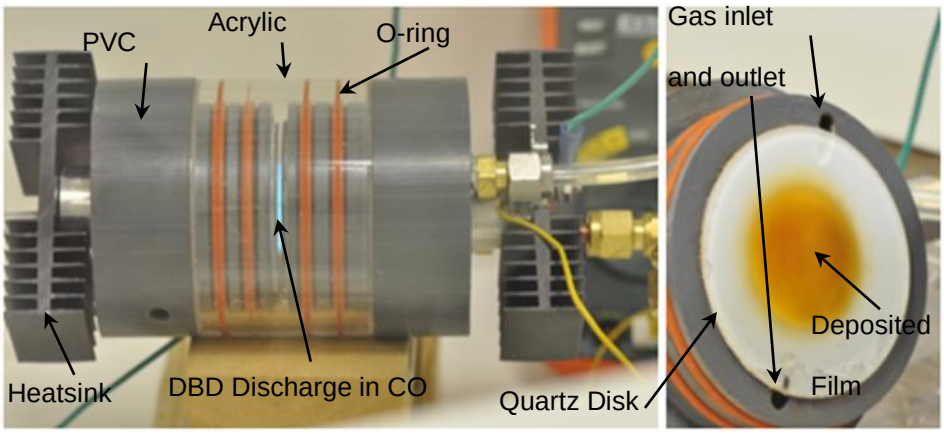

Figure 17 Experimental DBD reactor

3.4 Power Measurements

To determine the power of the plasma the voltage and current can be measured; a typical waveform is shown in Figure 18. Due to the streamers that are present in the dielectric barrier discharge (DBD) the current waveform has characteristic spikes which need to be considered for an accurate measurement of power. A common method for measuring the power of a DBD is generate Lissajous curves. Alternatively the power can simply be measured by multiplying the current and voltage over several periods. Both of these methods were used and compared. The difference between the two methods was negligible and therefore the simpler method, the latter method, was used to determine the power.

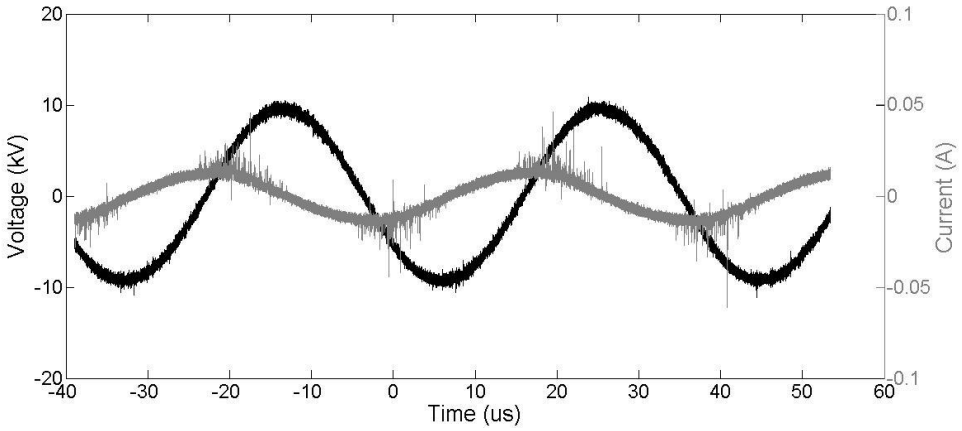

Figure 18 Voltage and current characteristics of the discharge

4. EXPERIMENTAL RESULTS*

4.1 Plasma Parameters

The plasma was generated with a 25 kHz sinusoidal signal of about 10kV peak voltage as shown in Figure 6. These current and voltage characteristics are comparable to characteristics of planar DBD discharge operating in high pressure molecular gases (such as air). The power supply is capable of supplying 200W however typical power inputs were around 10W corresponding to power densities on the electrode of about 2 W/cm^2. Increasing the power effectively increases the average power density within the reactor, as the electrode area remains constant. This increase in power density can affect the density of excited species and the gas temperature which can play an important role in the chemistry that takes place. The initiation mechanism for the chemistry that takes place in the plasma is thought to be either electron impact excitation of carbon monoxide, electron impact dissociation of carbon monoxide or some combination of the two. The initiation mechanism will be a function of the electron distribution function which depends on the power density. It may therefore be possible to have some control of the initiation mechanism simply by adjusting the power. Power adjustments will also affect gas temperature which in turn may affect product formation as discussed in the prior thermodynamics section.

In order to estimate the temperatures and the non-equilibrium nature of the plasma optical emission spectroscopy was carried out. The experimental emission spectrum of the carbon monoxide plasma is shown in Figure 20**(a)**. As can be seen the visible spectrum is rich with information about the species present and state of the plasma. In order to identify the vibrational

* Part of the data reported in this chapter is reprinted with permission from Geiger, R., Staack, D., *Analysis of Solid Products Formed in Atmospheric Non-thermal Carbon Monoxide Plasma* Journal of Physics D: Applied Physics, 2011. **44**(27) by IOP Publishing Ltd

band heads of various transitions spectral models were created for the C2 ($d^3\Pi \rightarrow a^3\Pi$) Swan bands as well as for the CO Angstrom ($B^1\Sigma^+ \rightarrow A^1\Pi^+$) and Herzberg bands ($C^1\Sigma^+ \rightarrow A^1\Pi^+$). These transitions emit light in the visible range making them useful for emission spectroscopy. The Herzberg band emission is around ~375 nm and the Angstrom band emission is around ~460 nm based off the energy difference of the bottom of the respective potential wells; the transitions that make up these bands are illustrated in Figure 19. Both the Angstrom and Herzberg bands are $\Sigma^+ \rightarrow \Pi^+$ transitions so they follow the same selection rules. The dissociation energy of carbon monoxide in its ground state is about 11.091 eV which is lower energy than the bottom of the potential well of the $C^1\Sigma^+$ state, which is about 11.35 eV. This means that the Herzberg bands might be difficult to detect in the emission spectra. The potential well of the $B^1\Sigma^+$ state is at 10.74 eV and the $A^1\Pi^+$ state is about 8.04 eV. Therefore the Angstrom band is expected to be quite detectable. The equilibrium separation for the $B^1\Sigma^+$ and $C^1\Sigma^+$ states are 1.120 Å and 1.122 Å respectively. Due to the similarity in these equilibrium separations the most probably transitions to the $A^1\Pi^+$ state should be very similar for both Angstrom and Herzberg bands. Molecular constants and Frank-Condon factors for these transitions were found in the literature [41,42, include Herzberg ref].

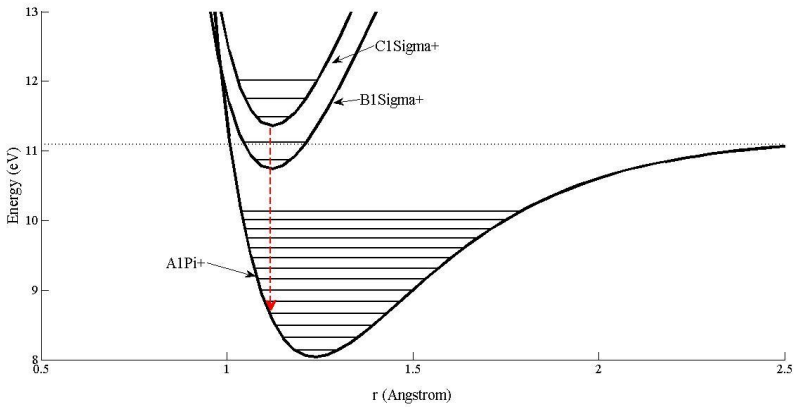

Figure 19 An illustration of the excited states of carbon monoxide that were modeled. The red arrow indicates the most probable transition according to the Franck-Condon principal. The dotted indicates the dissociation energy of carbon monoxide from its ground state

The models, evaluated at T_{vib} = 2000K and Trot = 400K are shown for comparison in figure 7(b-d). While the majority of features are described by these species and transitions there are several transitions between the wavelengths of 420-650 that are not identified. Most notably are the peaks around 438, 446, 468, and a small peak at 589. Dicarbon monoxide (C_2O) and dicarbon monoxide anion (C_2O-) have several transitions within the visible range that may explain some of these peaks [41]. Fitting the model to the experimental data can provide an estimate of the rotation and vibrational temperatures of the plasma however due to multiple overlapping transitions this can become complicated. The C_2 (d3-a3, 1-0 and 2-1) band at around 474 nm was relatively isolated from other bands and used for temperature estimates. From the C2 Swan band fit seen in Figure 8 the temperature estimates are Trot = 408 K, T_{vib} = 1062 K, the method of fitting is similar to that used in prior works for the N_2 2nd positive system [44]. The non-equilbrium nature of the plasma is illustrated by the differences in the vibrational temperature as compared to the rotational temperature which is near room temperature. A comparison of the Angstrom CO bands to the experimental data indicates that the rotational temperature of CO may be closer to room temperature than that of C_2. Discrepancies may arise

from C_2* formation through dissociative processes or other processes which do not preserve the equilibrium ground state rotational temperature. More accurate temperature predictions, including electronic temperature, can be made if the Herzberg and Angstrom bands are fit to the data as well; however these spectral models have not yet been validated.

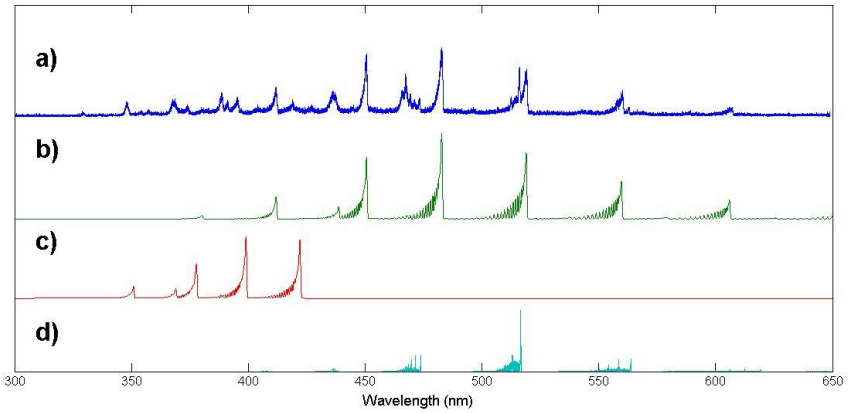

Figure 20 a) Experimental optical emission spectrum of the DBD carbon monoxide plasma b) Model of Angstrom CO Bands c) Model of Herzberg CO Bands and d) Model of C_2 Swan Bands Note: The models (b,c,d) shown were calculated at T_{vib} = 1200K and T_{rot} = 400K

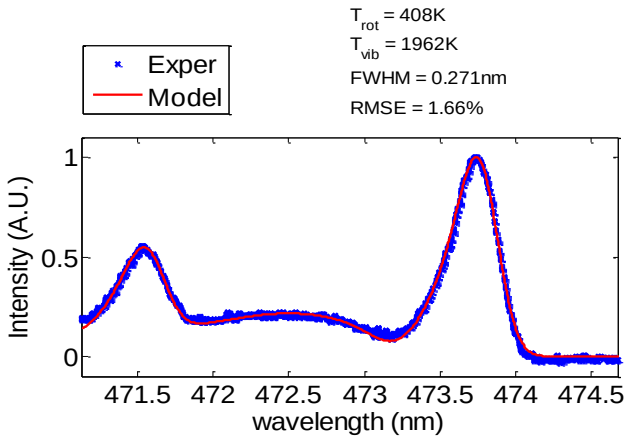

Figure 21 C_2 Swan Band C_2 ($d^3\Pi$-$a^3\Pi$) fit to the experimental data at the 2-1 and 1-0 transitions

4.2 Overall Kinetics

The overall kinetics of the system is analyzed by measuring the mass of depositions as a function of time, flow rate, gas temperature and power. The amount of material deposited as a function of time, for a constant power of 10 W, is seen to increase linearly, Figure 22. This indicates an approximately constant deposition rate of 0. 2 mg/min. The amount deposited was determined by measuring the mass gain on the removable quartz dielectric barrier and multiplying by 2 (assuming both electrode surfaces had similar film thickness). At short durations, less than one minute, the film is completely transparent and slightly longer durations will be transparent but have a yellowish hue. If the deposition is carried out for times above one minute the films range from yellow to brown depending on the discharge power. Inset pictures on Figure 22, are corresponding images of the deposited films. Thickness of these films are on the order of 1.4 μm after 10 minutes. As the film grows in thickness on the dielectric surface the gap will become smaller which may affect the plasma discharge. Furthermore the film itself will affect the conditions of the plasma according to the electrical characteristics of the deposited films. However with these considerations in mind, for the conditions that the experiments were run, that is as long as twenty minutes with an initial gap length of two millimeters and powers ranging from eight to twenty watts, no significant changes in operating conditions were observed.

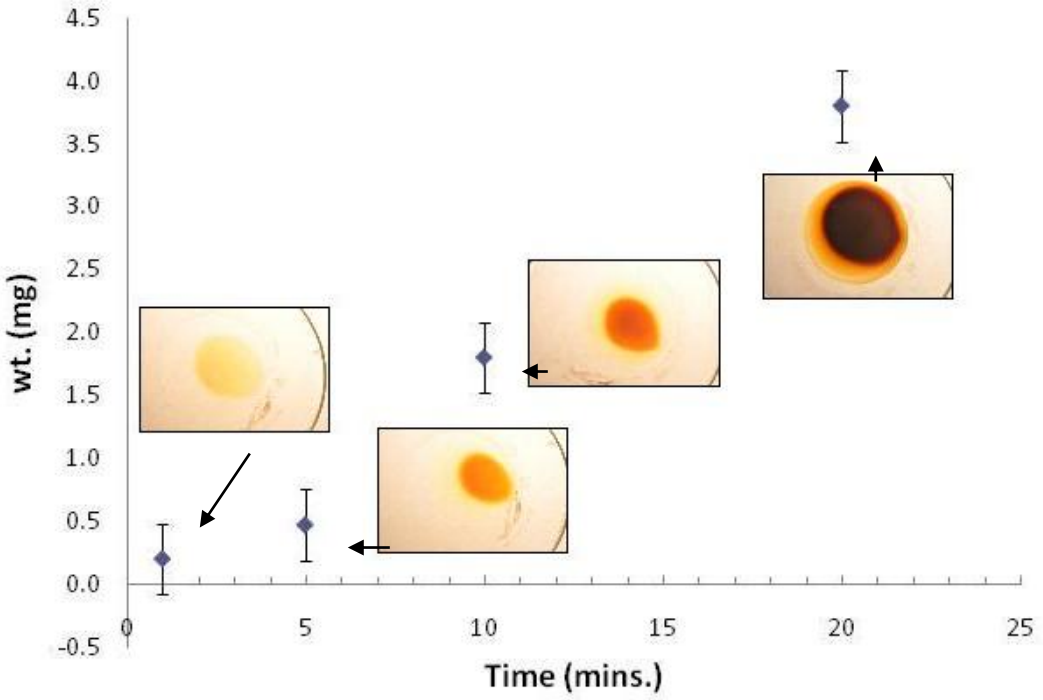

Figure 22 Rate of deposition plotted verse time a power of 10W and a flow rate of 0.5 SLPM

It has been determined that flow rate does not seem to play a significant role for the conditions under investigation, see Figure 23. This is most likely because there is only a small change in concentration of the deposition precursor (CO in this case) and the residence time of species in the plasma is quite long. At the lowest flow that is used in our experiments less than 0.1% of the carbon monoxide was converted to carbon suboxide and even smaller at higher flow rates. The flow rates of carbon dioxide in the exhaust are also measured to be less than 0.1%. These are not large conversion and some inefficiency in reverse reactions to CO are likely, conditions also were not optimized. In order to see the significant changes in chemical composition flow rates would have to be only a few milliliters per minute which is difficult with the current setup. In contrast to have residence times sufficiently short to affect chemical

reactions supersonic flow velocities or reduction of the discharge to the micro-scale would be required. These extreme effects were not studied.

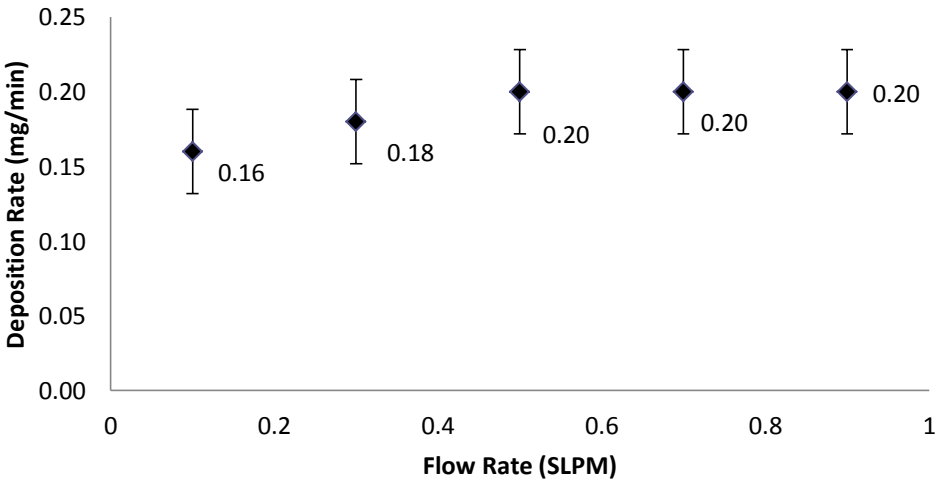

Figure 23 Deposition rate plotted verse flow rate

The power and the temperature tend to be important variables as anticipated from the previous thermodynamic and kinetic calculations. Deposition rate as a function of power is shown in Figure 24. It can be seen that the deposition rate increases with increasing power. Deposition rates were recorded at constant flow rates of 0. 5 SLPM and the runs were ten minutes in duration.

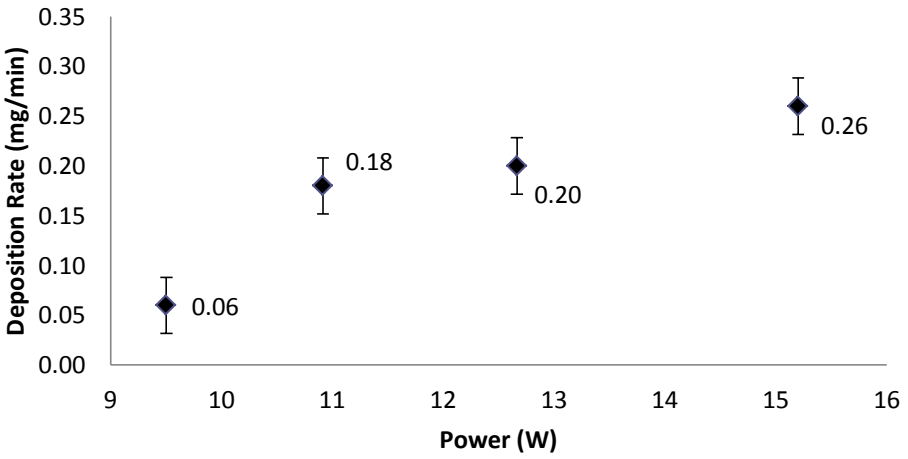

Figure 24 Deposition rate plotted verse power at 0.5 SLPM for 10 minute runs

During the experiments the temperature measured at exhaust line always increased, due to the power addition from the plasma into the reactor as well as possible exothermic reactions taking place. The increasing temperature with time for these measurements is show in Figure 25. Because it was difficult maintain a constant gas temperature in the atmospheric pressure DBD with increasing power or time it is difficult to experimentally isolate the effects of power and temperature. To get some idea regarding the effect of temperature on deposition rate the inlet gas temperature was increased. Increasing the inlet gas temperature to 50^{o}C caused the deposition to consist partially of a dark powder resembling graphite and could be wiped off while the normal low temperature films cannot be wiped off. Only a solvent such as water or ethanol can remove the lower temperature deposits. From the previous thermodynamic and kinetic analysis it was predicted that the carbon suboxide production is favored at lower temperatures and this appears to be consistent with these experimental results. Lower temperatures and lower power settings tend to favor a more yellow film while higher temperatures and higher powers produce darker brown films and even dark black powders.

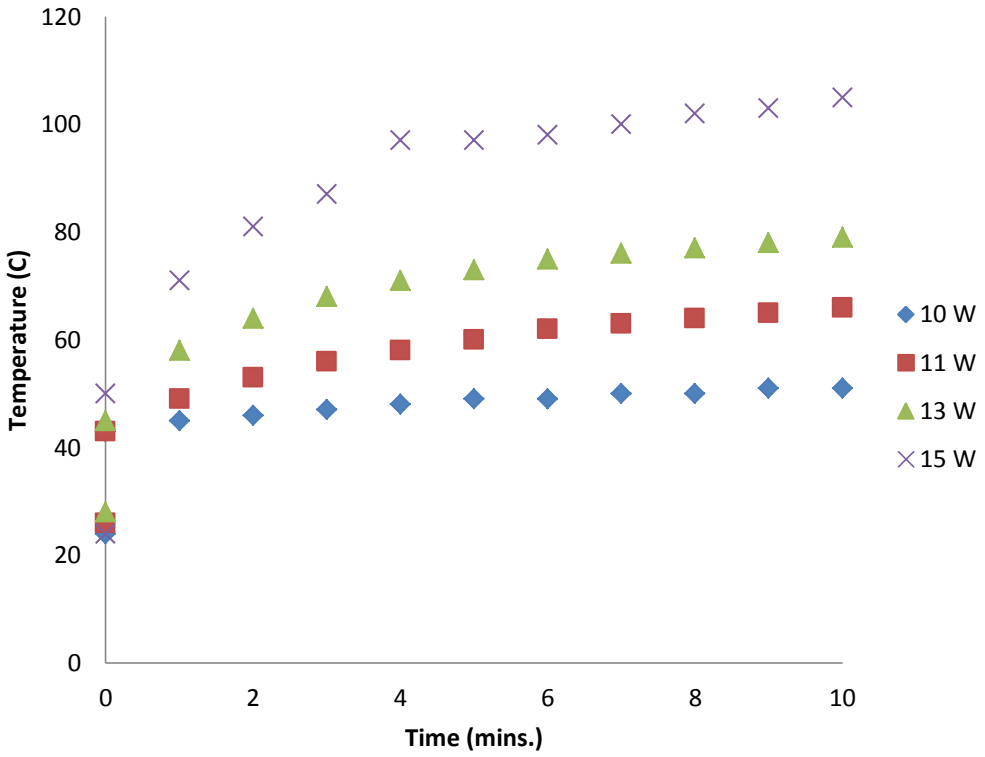

Figure 25 Gas temperature leaving the plasma verses time for various powers

Color variations in the deposition could be noted when operating the system depending on the flow rates and powers, a typical variation is shown in Figure 26. The region near the gas inlet is lighter and yellower in color which the region closer to the outlet is darker and browner in color. Insight into this unique deposition pattern can be explained by modeling the temperature and gas flow within the reactor using Comsol™. Here we have assumed a simplified 2D geometry, with uniform gas inlet, constant pressure outlet, and heat conduction at the reactor circumference proportional to the local temperature above ambient. If it is assumed that the plasma is heating the gas uniformly then the temperature in the region of the darker film will be higher, as shown in Figure 26b, which results in the observed deposition pattern. Therefore the darker films may be explained solely by temperature. Variations in power density

may also potentially explain the observed variations. Such variations may occur due to the convective flow or as a result of the non-uniform temperature and density distribution (assuming constant pressure). The variation in power density should be proportional to the temperature gradient, and $\Delta T/T$ is approximately 10% in the discharge region from the model. Further verification of potential power density variations was made by capturing high resolution images of the discharge, Figure 27(a) (being careful to use exposure times which do not saturate the CCD on the camera). Areas of higher power density would be expected to emit higher intensities of light from that area. Averaging several images plots of the intensity appears to be slightly non-uniform with brighter regions near the exit, see Figure 27(b) which corresponds to the image in Figure 27(a). The integrated intensity is about 12% higher on the right portion of the image. This, and the temperature estimates, suggests a power density non-uniform of only about 10-12%, comparable to an increase of about 1.2 Watts on Figure 26. In the previously mentioned power variation experiments such small power variations did not result in such a significant change in film color and therefore it seems as though temperature is responsible for the darker films. Such dependence is also justifiable since power density variations are linear with temperature whereas chemical kinetics typically varies exponential with temperature (see Figure 13 for example).

a)

b)

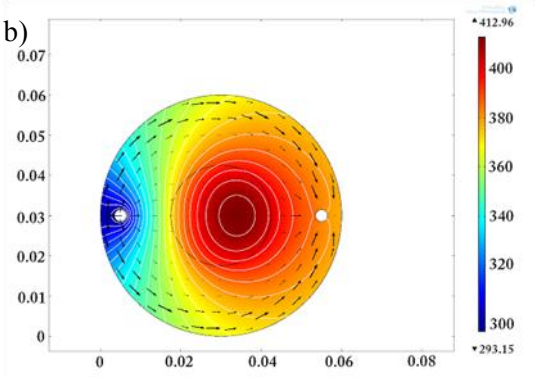

Figure 26 a) Variance of film color within the DBD. b) Comsol model of the flow within the DBD assuming uniform heating of Q = 500 W/m^3

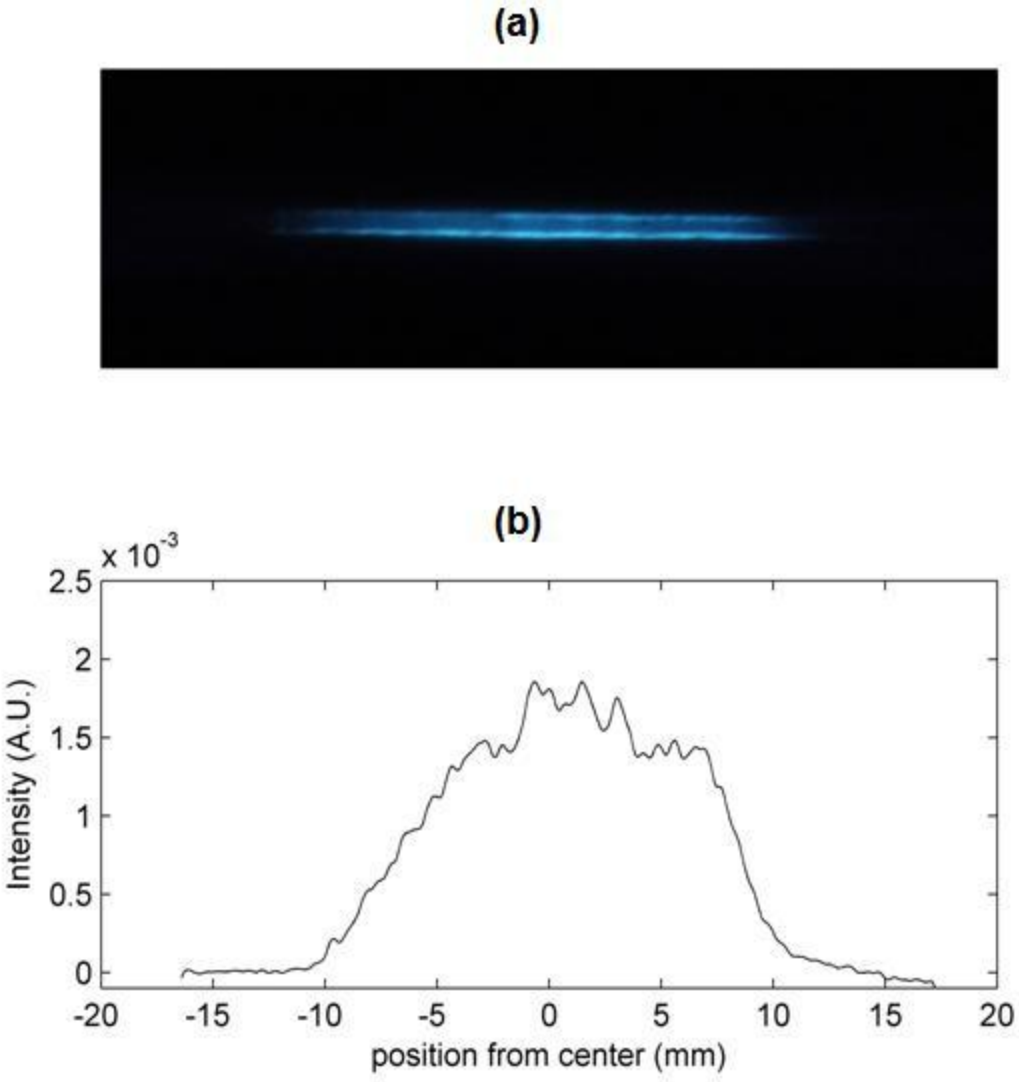

Figure 27 Figure 28 a) Picture of CO plasma from a side view b) Intensity plot of picture

4.3 Characterization

Characterization of the solid products formed from the carbon monoxide plasma may help to provide information regarding the mechanisms that take place within the plasma as well as information regarding the possible uses for the films. For many characterization techniques the film would have to be put into solution therefore several test of solubility were made. The films

were soluble in water, acetone, ethanol and DMSO forming a yellow to brown solution; some of the films were not completely soluble while others were, this seemed to depend on both the power and temperature for which the film was made. Generally only darker colored films had insoluble components. It seems conceivable that the insoluble portion was the more carbonaceous portion of the film as the lower power and lower temperature films were completely soluble.

X-ray photoelectron spectrometery (XPS) was carried out for several samples to try and understand the composition of the films, the structure of the films, and to see how the films change after they are put into solution. It is important to note that the XPS technique can only determine the structure and composition near the surface and may not reflect the properties of the overall substance; however it can still provide valuable information. Initial measurements were made to compare the ligher yellowish colored films with the darker brownish films; the compositions that were determined by this analysis are shown in Table 8 and the XPS for the carbon peak of the yellow sample is shown in Figure 29.

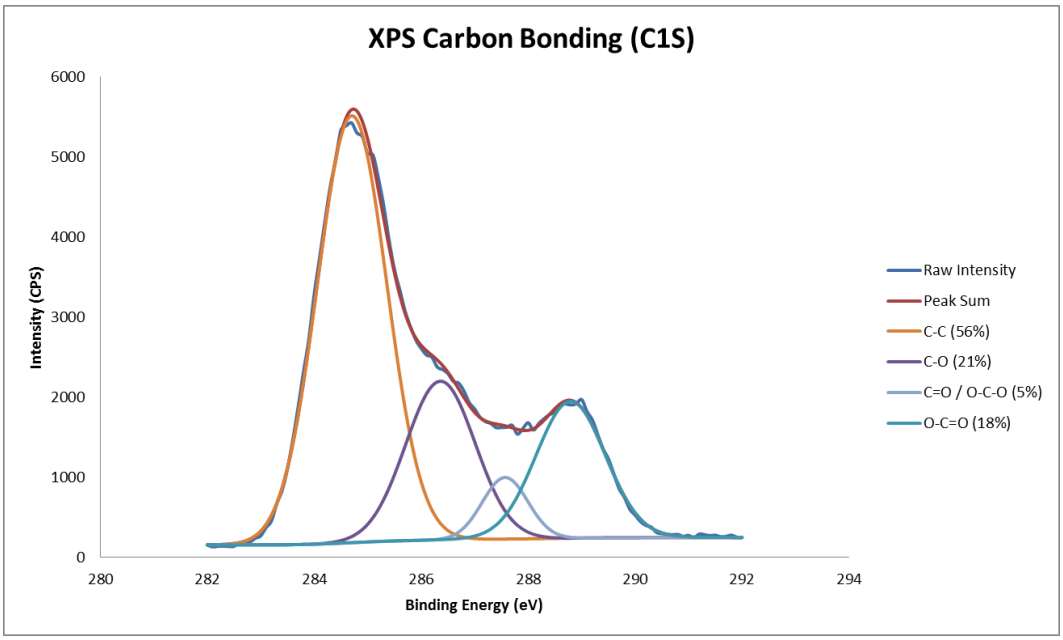

Figure 29 XPS of yellow solid product

It can be seen that the yellow films have a C/O ratio that is closer to what would be expected for pure carbon suboxide while the darker film tends to have more carbon.

Table 8 Composition as determined by XPS

Sample	C (%)	N (%)	O (%)	C/O
Pure Carbon Suboxide (Expected)	60.00	0.00	40.00	1.50
Yellow	64.10	3.40	32.50	1.97
Redish-Brown	66.63	14.06	19.31	3.45
Non-hydrolyzed	59.01	2.23	36.31	1.63
Hydrolyzed	61.48	1.59	36.60	1.67

Samples were also produced of a red-brown color and these samples were scraped from the quartz disk to which it was deposited and a portion of this sample was measured directly using XPS while the other portion of the sample was put into an aqueous solution and then extracted through evaporation and subsequently measured using XPS. Figure 30 shows a distinct change in color before and after the solid product was hydrated.

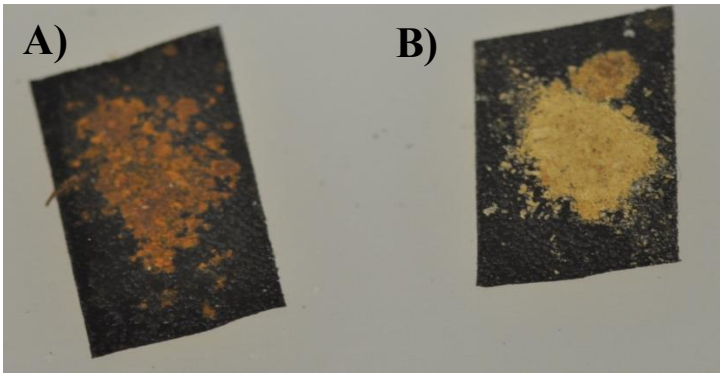

Figure 30 Visual comparison of A) Solid sample before being put into solution B) Solid sample after being put into an aqueous solution

The XPS results for the carbon peak of both samples are shown in Figure 31. Two distinct differences are seen between the two samples. As seen in Table 8 the C/O ration only changed slightly resulting in a slightly higher concentration of carbon; however upon inspection of the carbon peaks it is apparent that the bonding has changed. The peak around 286.5 eV increased after reaction with water. In general this peak is attributed to a C-O bond which would imply that the reaction with water increases the concentration of C-O bonding that is taking place. At the same time there is a decrease in the peak near 289 which may be attributed to a C=O C group.

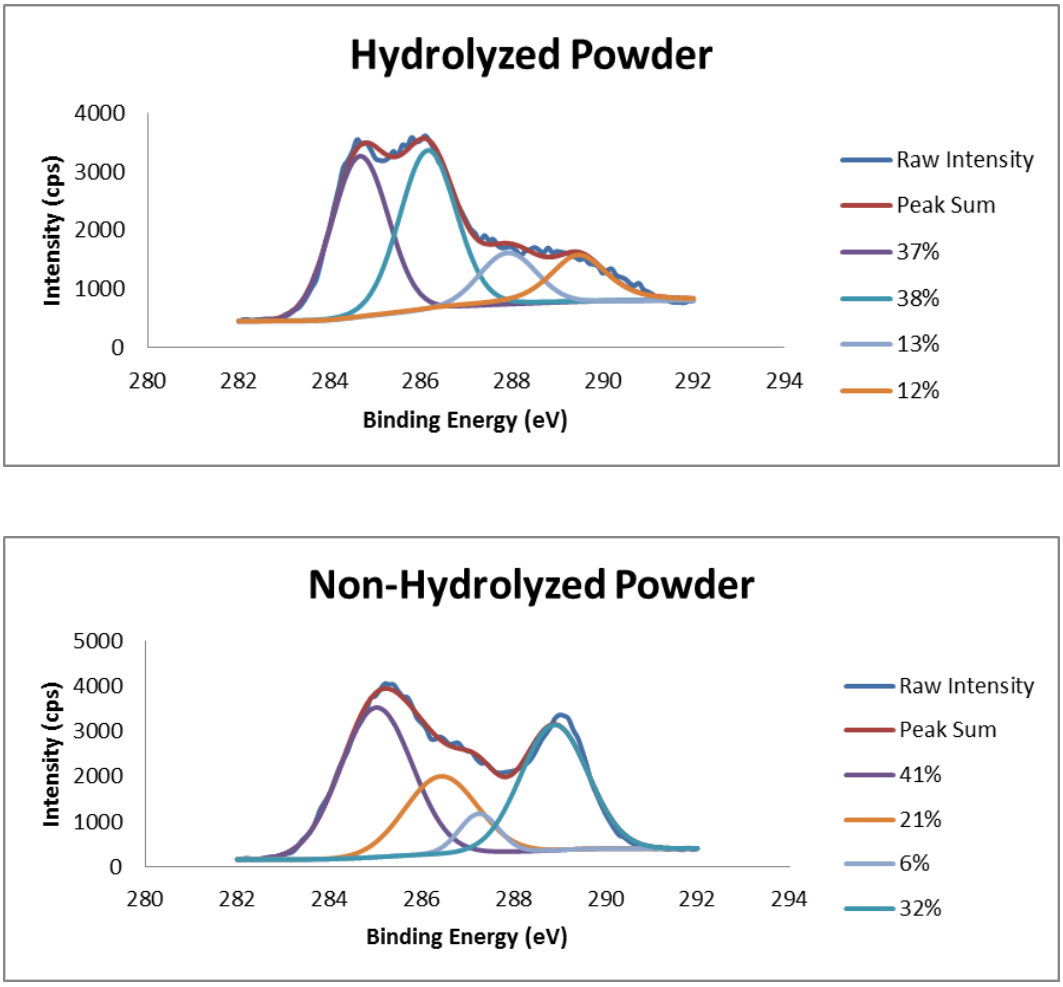

Figure 31 XPS results for solid products before (Non-Hydrolyzed Powder) and after (Hydrolyzed Powder) the solid products were put into an aqueous solution

The samples to be analyzed were scraped from the quartz dielectric surface to which they had been deposited. Samples were sent out for elemental analysis to Midwest Microlabs using combustion at 990^{o}C followed by an elemental analyzer to determine CHN and pyrolysis at 1200^{o}C to determine O gravimetrically. The results of the elemental analysis provide the following mass percentages: 41% Carbon, 3% Hydrogen, 51% Oxygen 0.4% Nitrogen and 4.5% Ash. The ash concentration is most likely some form of graphitic carbon remaining from the

elemental analysis procedure. With this assumption in mind the resulting mole percentages would be $C_{0.38}H_{0.30}O_{0.32}$. However if the assumption that the ash is not carbon and the ash is ignored concentration the composition would be slightly different, $C_{0.36}H_{0.31}O_{0.33}$. These results contain an unexpected amount of hydrogen present in the samples.

The possibility that water may have simply absorbed into the material was tested when a second sample was dried under vacuum at 110^{o}C before the elemental analysis, however the results were the same concentrations and therefore the hydrogen was not due to absorbed water. It was therefore thought that the source of hydrogen available to the sample is reaction with water present in the atmosphere while the sample had been exposed to air during the scraping process. Changes to the chemical structure of C_3O_2 upon exposure to water vapor in the air have been documented previously, [26, 53] although elemental mass analysis was not performed in those studies. Another possibility is that the hydrogen in the sample can come from impurities in the carbon monoxide, however this seems unlikely considering the mass of hydrogen which was deposited. An estimate of this is made by considering that the bottled carbon monoxide has a purity of 99.999% which is equivalent to 10 ppm of impurities. Based on a deposition rate of about 0.2 mg/min and the hydrogen mass fraction the amount of hydrogen present in the solid samples is equivalent to about $7x10^{-5}$ SLPM of hydrogen. For these conditions the incoming carbon monoxide flow rate was 0.5 SLPM. Therefore the necessary concentration of hydrogen impurity in the carbon monoxide is estimated to be around 140 ppm, this makes the strong assumption that all of the hydrogen impurity is converted into the solids. Even so this is 14 times higher than the expected impurities. The 10 ppm impurities which are expected to be present in the CO could conceivably in an extreme case lead to an atomic fraction of 2% hydrogen; however, this is significantly less than the 31% measured. We also do not believe that water vapor or air leaked into the vessel as it was pressure tested to 40 psi and was operated at 1-

2 psi above ambient pressure, preventing inward air leaks. The conclusion is that the deposited solids are extremely hygroscopic, not only absorbing but also reacting with the water from the air. Assuming all of the hydrogen came from water and correcting for it results in a carbon to oxygen ratio of 2.3 or 2 if we do not include the ash. This of course also assumes negligible losses of carbon and oxygen when the sample reacted with the water. If carbon and oxygen is lost during the reaction with water it would most likely be in the form of carbon dioxide resulting in a slightly lower oxygen concentration. If the original film, prior to exposure, was indeed carbon suboxide it would have had a carbon to oxygen ratio of 1.5. The high carbon composition in the sample could in fact be explained by a stoichiometric release of carbon dioxide when reaction with water. Though not conclusive, results from the elemental analysis indicate carbon suboxide as a possible original film (prior to air exposure). This is further supported by the fact that carbon suboxide is known to be extremely hygroscopic as well [28, 97]. Although attempts were made to avoid exposing the samples to water this feat proved difficult due to the large sample size required for analysis and while using the current setup; therefore all of the results from characterization experiments should be assumed to be of exposed films.

Figure 32 shows results from solid state NMR carried out on the samples using two methods and several interesting peaks were observed. The C-MAS NMR quantitatively indicates all bonds while the H decoupled only shown non-hydrogen bonds. From the carbon chemical shifts the first observation that could be made was a very broad peak that spanning the spectrum which can be described by the existence of an underlying resonant aromatic structure. Other peaks are comparable to the peaks observed by Schmedt auf der Gunne et al. [97] for carbon suboxide polymer; they report four major peaks at 96, 107.5, 150 and 163 which account for 95% of the total spectrum. It is further suggested that these peaks represent two different carbon

environments: carbon bonded to two carbons and one oxygen atom, and carbon bonded to one carbon and two oxygen atoms. It is conceivable that the broad peak at 165.9 seen in Figure 32, which spans from 150 to 175, corresponds to the peaks 163 and 150. This peak is the dominant peak in the spectrum and should constitute the basic structure of the solids which we deposited. The peak at 100.8 is not a common peak for carbon however may be a blending of the 107.5 and 96 peaks observed in the carbon suboxide spectrum. Peaks at 20.6, 11.2, and 2.4 suggest sp3 bonds such as methyl groups or some kind of saturated hydrocarbons exist. By comparing to the proton decoupled image we notice an unusually sharp peak at 132.2 and 122.5 which should correspond to sp2 bonds. The presence of methyl groups, or saturated hydrocarbons, in the film is quite interesting and hydrogen in the discharge would seem to be a proper explanation for their presence; however as mentioned although some trace impurities are present it does not seem likely that such a significant amount of hydrogen in present in the discharge. Therefore methyl groups and saturated hydrocarbon formation should also be considered. In order to explain this one can assume that pure carbon suboxide polymer is formed in the discharge and no hydrogen is present prior to exposing it to air. If this assumption is correct then it is important to realize the structure of this polymer will have very reactive terminating ketene groups (R'R''C=C=O). Reactions with these functional groups can effectively degrade the polymer. It is therefore conceivable that when the pure sample is exposed to air, or more specifically humidity, there may be some reaction pathways that are capable of producing small concentrations of methyl groups and saturated hydrocarbons. These sp2 and sp3 bonded hydrogen are notable in the NMR due to their sharp peaks however the area of these peaks is small compared the total spectrum area (<5%) and quantitatively these bonds represent a small fraction of all the bonds. From further analysis of the NMR, similarities exist between carbon suboxide polymers and the solid deposits we made however there are several differences: the peak at 165.0 is much larger

than the peak at 100.8 whereas for the carbon suboxide polymer spectrum the opposite was true, the sharp peaks at 132.2 and 122.5 do not exist for carbon suboxide polymer, and the other peaks below 80 do not show up for carbon suboxide polymer. Such differences between plasma polymerized films and other polymerization techniques are common. Plasma films are generally known to be more disordered, thus the significantly broadened peaks. Overall these NMR results indicate a film with similarities to polymeric carbon suboxide, but also with significant aromatic structures, hydrocarbon characteristics and hydrogen incorporation.

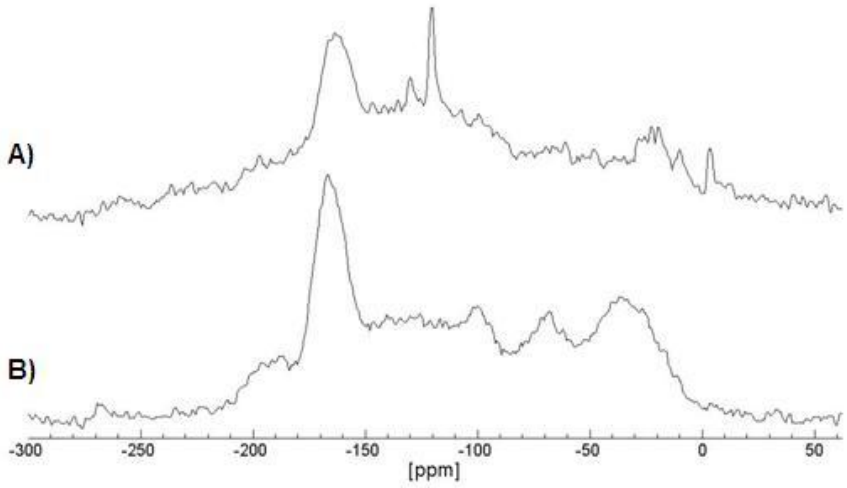

Figure 32 Solid State ^{13}C-MAS NMR of solid deposition: A) CPMAS B) H decoupling

Functional groups of the samples were analyzed using Fourier Transform Infrared Spectroscopy (FTIR). A comparison was made between samples yellow in color, resulting from relatively low power, and samples brown in color, resulting from higher power and is shown in Figure 33. The FTIR analysis showed very similar functional groups between the brown and yellow samples. A prominent peak is observed at 1734 cm^{-1} which can be assigned as a carbonyl

group; this observation was also observed from the NMR as well. The sideband at 1630 cm^{-1} shows the presence of double bonds. The peak at 1400 cm^{-1} can be –C-(C=O)-O-and at 1210 cm^{-1} –C-(C=O)-C-which are peaks that are to be expected to exist in carbon suboxide polymers. A peak at 2370 cm^{-1} is commonly observed in carbon suboxide and is considered to be a ketenyl band [28]. It has been shown that this peak tends to disappear with exposure to water while a second peak at 2336 cm^{-1} appears [97]. A comparable peak at 2340 cm^{-1} is observed in Figure 33 and is more intense for the yellow film and actually has a second less intense peak near it at 2362 cm^{-1}. Many of these peaks are also consistent with the results present by Lipp [48] for high pressure CO products with the exception of the 2340 cm^{-1} peak; it was also suggested by Lipp that the broad peak at 3400 cm^{-1} is not only due to –OH but the result of second harmonics or combinational bands of C=O and C=C stretching modes. Lipp mentions that his films are very similar to carbon suboxide but pointed out that the 806 cm^{-1}, 1365 cm^{-1} and 1511 cm^{-1} peaks typically seen in carbon suboxide are missing in his spectra. In the spectra for our yellow film shown in Figure 33 the peak at 806 cm^{-1} can be seen, which is considered a strong band of C_3O_2, however this peak is not as noticeable in the brown film spectrum. In relations to the two other peaks which concerned Lipp, Snow demonstrated [28] that for carbon suboxide the peaks near 1365 cm^{-1} and 1511 cm^{-1} region tend to broaden and become indistinguishable as a result of water exposure. Overall these FTIR results indicate that the plasma deposited films are similar to but not identical to carbon suboxide. More disorder features similar to the high pressure CO polymers of Lipp are also observed. Also clearly observed here is that the darker colored films produced by the plasma at high powers are less like carbon suboxide (based upon the 806 cm^{-1} peak). Reaction of the film indicative of exposure to water vapor is also indicated in the FTIR.

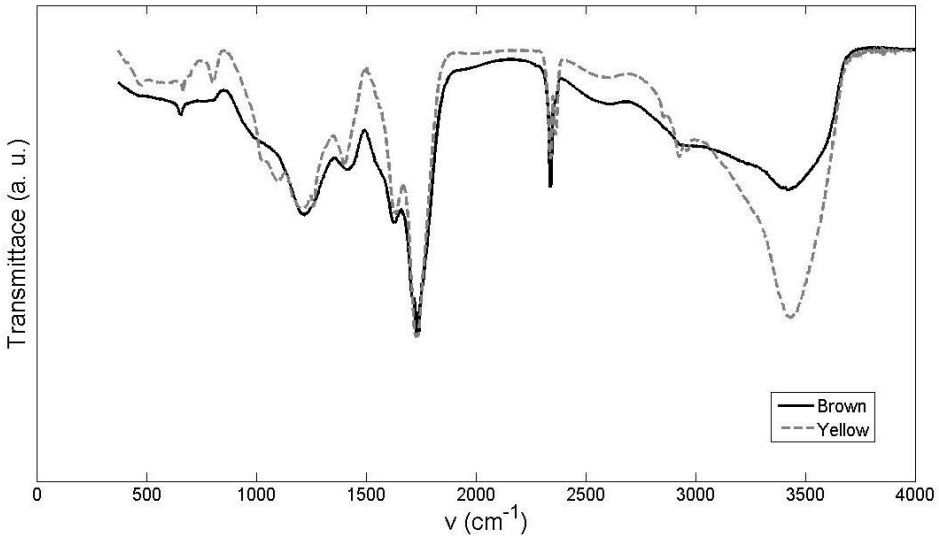

Figure 33 FTIR of brown and yellow films

The final analysis carried out on the samples was Matrix-assisted laser desorption/ionization (MALDI) and Electrospray ionization (ESI) mass spectrometry. These soft ionization techniques are able to prevent fragmentation providing the ability to detect larger molecules. Using these techniques a variety of peaks were observed below 500 amu (or Daltons) as can be seen in Figure 34b. In the higher range broad peaks near 2000 amu were observed. Of the larger masses recorded, a peak 1933.6 amu can be seen in Figure 34a. The broadness of the peaks suggests that the species are multiply charged, which is common when using ESI, and may therefore be several times larger than 1933.6 amu. Using MALDI, which typically does not result in multiply charged molecules, scans were taken up to 10000 amu with no detectable species. This further suggests that the multiply charged species at 1933.6, observed with the ESI, are most likely greater than five times multiply charged to have a mass larger than 10000 amu. If the species are polymers of carbon suboxide then multiples of C_3O_2 molecular weights, $(68)_n$, should be expected. Proceeding with this assumption, the spacing between groups around

1933 would correspond to 14 multiple charges, molecular weights on the order of 27,000 amu and polymer length of about 400 units. The broadness may be attributed to slight differences in atomic weight depending on the ways in which the polymers terminate. It is possible that the polymer terminates with a ketene, a very reactive termination, which would not alter the molecular weight from its monomer multiples. Another possible termination is a hydroxyl group. The mass spectroscopy results show that molecules, other than multiples of carbon suboxide, exist. These molecules could be explained as products of carbon suboxide reacting with atmospheric moisture or simply other products created in the plasma. The low weight peaks are expected to be interactions of the film with the solvent used in the technique.

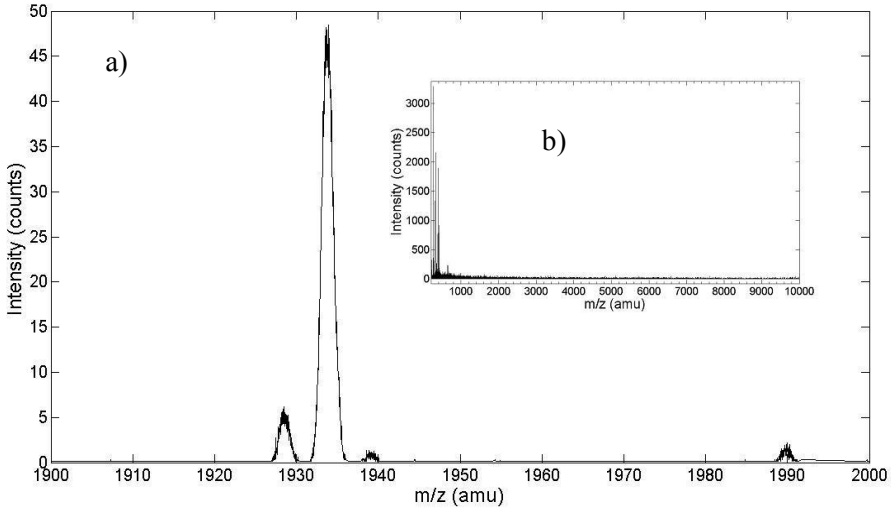

Figure 34 a) ESI + Mass Spectrum analysis showing multiply charged species around 1933.6 amu. b) Maldi Mass Spectrum analysis showing small molecular weights but no species up to 10000 amu

5. CONCLUSIONS AND FUTURE WORK

5.1 Summary

The goal of this thesis was to analyze the synthesis of carbon suboxide using a carbon monoxide plasma. This analysis involved a complete literature review of carbon suboxide, presented here chronologically as a history of carbon suboxide. From the literature thermodynamic properties were obtained and used to analyze various equilibrium and pseudo-equilibriums among oxides of carbon. Furthermore relevant kinetic data obtained from literature was compiled and compared to better understand the process by which carbon suboxide can form; this ultimately led to a proposed mechanism. An experimental setup was constructed for the purpose of synthesizing carbon suboxide using a dielectric barrier discharge (DBD). Optical emission spectrums were used to determine plasma properties such as temperature by comparing experimental data to the models generated by the Matlab code provided in the appendix. Experiments were carried out and mass and energy balances were made on the system which provided deposition rate information and energy cost information. The material formed in the DBD was characterized by FTIR, NMR and Mass Spectroscopy in order to determine if carbon suboxide was created.

5.2 Work Accomplished

The work accomplished throughout this research was a combination of both theoretical and experimental research. In terms of the theoretical research that has been accomplished several models were created. These models are:

1) A thermodynamic equilibrium simulation
2) Kinetic simulations

3) Optical emission spectrums of two excited states

4) Heat transfer model of the reactor

The experimental accomplishments involved the design and construction of several prototypes for the dielectric barrier discharge reactor which ultimately led to the reactor describe in this thesis. The reactor was used to successfully produce solid products. A complete characterization of the reactor was obtained through power measurements. Several methods of characterization were carried out on the solid products.

5.3 Major Findings

It has been determined experimentally that nonthermal carbon monoxide plasma produces a solid product at ambient conditions. It was further determined that this solid product has many similar features and characteristics to carbon suboxide polymer. Productions rates were on the order of 0.2 mg/min with power consumption on the order of 10W. Increasing temperature seems to make the product have darker color and is more powdery; from this result and from FTIR analysis it seems that higher temperatures tend to produce more carbon which is consistent with the thermodynamic and kinetic analysis.

5.4 Conclusions

Solid products formed in an atmospheric nonthermal carbon monoxide plasma were investigated. Thermodynamic calculations illustrate that solid oxides of carbon are more stable products then carbon monoxide at low temperatures. A simplified kinetic calculation shows that solid polymeric carbon suboxide can form faster than solid carbon under vibrational non-equilibrium of carbon monoxide. This type of non-equilibrium state can be created using nonthermal plasma. It was shown that solid depositions could be made in a nonthermal carbon monoxide DBD plasma at atmospheric conditions. The optical emission spectrum from the

plasma consist of CO Angstrom bands, C_2 Swan bands and CO Herberg bands; however other peaks exist that may be attributed to transitions of the dicarbon monoxide molecule. The overall kinetics of the process was explored and important trends were determined. The formation of solid carbon oxides is favored at lower power densities and lower temperatures as predicted from the previous thermodynamic calculations. Although deposition rates increase with increasing temperature it was seen that the depositions become darker and can even become powdery with higher carbon concentrations.

The solid deposits were characterized in order to determine whether carbon suboxide is being generated. Although it has not been completely determined whether carbon suboxide is originally deposited from the plasma, mainly due to the difficulty inherent of the hygroscopic and reactive nature of the material, much of the results suggest a good possibility that it is; most notably is the existence of the 806 cm^{-1} peak in the IR spectra as well as the 2336 cm^{-1} which also appears in carbon suboxide polymers that have been exposed to water; furthermore NMR data provide information regarding the structure of the depositions having some similarities to carbon suboxide polymer though generally appear more disordered. Finally, results of the mass spectroscopy analysis reveal that large molecules, greater than 10000 amu, exist within the films, this would indicate suboxide polymers with chain lengths greater than 150. Further confirmation of carbon suboxide formation can be had if experiments are carried out carefully, so as not to expose the samples to humidity, at low temperatures and low power settings.

5.5 Suggested Future Work

The mechanism that has been suggested by many authors in the literature, and by this thesis, for the production of carbon suboxide through carbon monoxide excitation suggests that carbon

suboxide monomer is produced in the gas phase and is then polymerized; however the current thesis only analyzed the solid products and was never analyzed the gaseous formation of carbon suboxide monomer. The monomer exists in the gas phase at room temperature however it condenses just above 6^{o}C. It is the opinion of the author that the plasmachemical production of carbon suboxide monomer in its liquid phase is possible and should be investigated. To avoid polymerization the carbon suboxide would have to be rapidly quenched out of the gas phase and should not be allowed to spend too much time in the plasma. This may be accomplished perhaps by simply cooling the pure carbon monoxide to a temperature, and more importantly the operating temperature of the gas, well below the condensation temperature of carbon suboxide. Alternatively the velocity of the carbon monoxide through the reactor can be increased to rates faster than polymerization would normally occur. Another option is to increase the pressure of operation in order to change the condensation temperature to above room temperature; reference can be made to the P-v diagram presented in Section 2. These experiments would lead to partial verification of the proposed mechanism and could prove to be a valuable method for the rapid production of carbon suboxide monomer in the lab and possibly on an industrial scale is so desired.

The proposed mechanism relies on the production of dicarbon monoxide however this radical has not be observed during the production of carbon suboxide. In order to further verify the proposed mechanism experiments can be carried out to analyze dicarbon monoxide production. There are well known absorption and emission lines that can be used to detect the radical and experiments can be designed accordingly.

The method and reactor used for the production of carbon suboxide in this thesis was not optimized and therefore further experiments can be carried out to optimize this process. The

resident time that was used was way too short to produce considerable amounts of the product. Further considerations can be made to the capacitive coupling of the discharge and the frequency and power of operation. Lastly, although some experiments were made to determine the effect of pressure and temperature on the production rates further experiments are required in order to better understand their influence.

REFERENCES

1. Diels O, W.B., *Ueber das Kohlensuboxyd. I.* Chemische Berichte 1906. **39**: p. 689-697.
2. C. Kunz, P.H., S. Dondes, *Mechanism for Excitation of the C2 High-Pressure Bands.* Journal of Chemical Physics, 1967. **46**(10): p. 4157.
3. Dondes, P.H.a.S., *Reply to the Letter to the Editor on ``Slow Reaction of Carbon Monoxide with Oxygen''. by R. H. Knipe and A. S. Gordon* Journal of Chemical Physics, 1957. **27**(6): p. 1419.
4. Dondes, P.H.a.S., *Reaction of Carbon Monoxide and Ozone.* Journal of Chemical Physics, 1957. **26**(6): p. 1734.
5. G. Liuti, S.D., and P. Harteck, *Isotopic Enrichment in the Photochemistry of CO with the 2062-A Iodine Line.* Journal of Chemical Physics, 1966. **44**(10): p. 4052.
6. G. Liuti, S.D., and P. Harteck *Photochemical Production of C3O2 from CO.* Journal of Chemical Physics, 1966. **44**(10): p. 4051.
7. G. Liuti, S.D., and P. Harteck, *The Photochemical Separation of Carbon Isotopes*, in *Isotope Effects in Chemical Processes*. W. Spindel, Editor. 1969, American Chemical Society: Greenbelt, Md. p. 65-72.
8. S. Dondes, P.H., H. von Weyssonhoff, *The Gamma Radiolysis of Carbon Monoxide in the Presence of Rare Gases.* Z. Naturforsch, 1964. **19a**(1): p. 13.
9. Brodie, B.C., *Note on the Synthesis of Marsh-Gas and Formic Acid, and on the Electric Decomposition of carbonic oxide.* Proceedings of the Royal Society of London, 1872-1873. **21**: p. 245.

10. Brodie, B.C., *On the Action of Electricity on Gases. II. On the Electric Decomposition of Carbonic-Acid Gas.* Philosophical Transactions of the Royal Society of London, 1874. **164**: p. 83.

11. Brodie, S.B.C., *An Experimental Inquiry on the Action of Electricity on Gases. I. On the Action of electricty on oxygen.* Proceedings of the Royal Society of London, 1872. **162**: p. 435.

12. Geiger, R., Staack, D., *Analysis of Solid Products Formed in Atmospheric Non-thermal Carbon Monoxide Plasma* Journal of Physics D: Applied Physics, 2011. **44**(27).

13. Pauling, L.O.B.a.L., *The Electron-Diffraction Investigation of the Structure of Molecules of Metyl Azide and Carbon Suboxide.* Proceedings of the National Academy of Sciences, 1933. **19**(9): p. 860-867.

14. Langmuir, I., *Chemical Reactions at Low Pressure.* Journal of American Chemical Society, 1915. **37**(5): p. 1139.

15. Langmuir, I., *Surface Chemistry.* Chemical Reviews, 1933. **13**(2): p. 147.

16. Berdahl, V.I.O.a.B.J., *A Model of Martian Surface Chemistry.* Journal of Molecular Evolution, 1979. **14**: p. 199-210.

17. Carsont, W.T.P.a.R.K., *Mars: Is the Surface Colored by Carbon Suboxide?* Science 1969. **166**: p. 1141-1142.

18. V. I. Oyama, B.J.B., F. Woeller,M. Lehwalt, *The Chemical Activities of the Viking Biology Experiments and the Arguments for the Presence of Superoxides, Peroxides, Gamma-Fe2O3 and Carbon Suboxide Polymer in the Martian Soil.* Life Sci Space Res., 1978. **16**: p. 3-8.

19. Perls, T.A., *Carbon Suboxide on Mars: A Working Hypothesis.* Icarus, 1971. **14**: p. 252-264.

20. Shimizu, M., *Ultraviolet Absorbers in the Venus Clouds.* Astrophysics and Space Science, 1977. **51**: p. 497-499.

21. Shimizu, M., *An Evolutional Model of the Terrestrial Atmosphere from a Comparative Planetological View.* Precambrian Research, 1979. **9**(3-4): p. 1979.

22. Moore, P.A.G.a.M.H., *Carbon Suboxide in Astrophysical Ice Analogs.* Icarus, 2001. **154**(2): p. 372-380.

23. T. Wesley Huntress Jr, M.A.a.M.D., *Carbon Suboxide in Comet Halley?* Nature, 1991. **352**: p. 316-318.

24. Shimizu, M., *Carbon Suboxide and the Genetic Code.* Astrophysics and Space Science, 1979. **62**(2): p. 509-513.

25. Shimizu, M. *Evolution of Atmosphere - Comparative Planetology*. in *Proceedings of the Second ISSOL Meeting and Fifth ICOL Meeting*. 1978. Kyoto, Japan: Center for Academic Publications Japan.

26. Egami, H.Y.a.F., *Is Carbon Suboxide a New Candidate as Starting Material for the Synthesis of Biomolecules on the Primitive Earth.* Precambrian Research, 1981. **14**: p. 75-80.

27. Ross, A.H.T.a.W.F., *Carbon Suboxide and Proteins.* Journal of Biological Chemistry, 1942. **146**: p. 63-68.

28. A. W. Snow, H.H., N. L. Yang, *Poly(carbon suboxide). Characterization, Polymerization, and Radical Structure.* Macromolecules, 1978. **11**(1): p. 77-86.

29. N. L. Yang, A.S., H. Haubenstock, F. Bramwell, *Poly(carbon suboxide): A Photosensitive Paramagnetic Ladder Polymer.* Journal of Polymer Science: Polymer Chemistry Edition, 1978. **16**(8): p. 1909-1927.

30. Sheahen, T.P., *Observation of C3O2 During Atmospheric Reentry* Combustion and Flame. 1974. **22**(2): p. 243-251.

31. M. L. Burke, W.L.D., P. M. Sheaffer, P. F. Zittel, and L. S. Bernstein, *Formation of Triplet CO in Atomic Oxygen Flames of Acetylene and Carbon Suboxide.* J. Phys. Chem., 1996. **100**(1): p. 138-148.

32. Bayes, K.H.B.a.K.D., *CO Chemiluminescence from Flames.* Journal of Chemical Physics, 1968. **48**(2): p. 653.

33. Gaydon, A.G., *The Flame Spectrum of Carbon Monoxide.* Proceedings of the Royal Society, 1940. **176**: p. 505-521.

34. Alexander Fridman, A.G.a.A.D., *CO2-Free Energy and Hydrogen Production from Hydrocarbons.* Energy Fuels, 2006. **20**(3): p. 1242-1249.

35. Matthias Ballauff, L.L., Sabine Rosenfeldt, Nico Dingenouts, Johannes Beck, Petra Krieger-Beck, *Analysis of Poly(carbon suboxide) by Small-Angle X-ray Scattering.* Angewandte Chemie International Edition, 2004. **43**(43): p. 5843-5846.

36. Brodie, B.C., *On the Action of Electricity on Gases [Abstract].* Proceedings of the Royal Society of London, 1871. **20**: p. 472-475.

37. Brodie, B.C., *The Induction Tube of W. Siemens.* Nature, 1874. **9**(225): p. 308.

38. Mumford, R.L.a.L., *The Decomposition of Carbon Monoxide in the Silent Electric Discharge - Part 3.* Journal of the Chemical Society, 1929: p. 1711-1723.

39. Mumford, R.L.a.L., *The Decomposition of Carbon Monoxide in the Corona due to Alternating Electric Fields - Part 1.* Journal of the Chemical Society, 1925. **127**: p. 2052-2057.

40. Mumford, R.L.a.L., *The Decomposition of Carbon Monoxide in the Corona due to Alternating Electric Fields - Part 2.* Journal of the Chemical Society, 1927: p. 857-867.

41. Schmidt, E.O.a.K., Chemische Berichte, 1922. **55**: p. 2126.

42. Nightingale, H.W.H.a.R.E., *Gas Cooled Power Reactor Coolant Choice*. 1958: Oak Ridge National Laboratory.

43. Chen, C.-C., *The Carbon Monoxide Laser: A Review*. R. Corporation, Editor. 1974: Santa Monica, California.

44. M. Lipp, W.J.E., V. Garcia-Baonza, and H. E. Lorenzana, *Carbon Monoxide: Spectroscopic Characterization of the High-Pressure Polymerized Phase.* Journal of Low Temperature Physics, 1998. **111**: p. 247-256.

45. R. Mills, D.S., A. Katz, B. Olinger, *New Phases and Chemical Reaction in Solid CO Under Pressure.* Journal de Physique Colloques 1984. **45**: p. 3176-3179.

46. Stephane Bernard, G.L.C., Sandro Scandolo, and Erio Tosatti, *Decomposition and Polymerization of Solid Carbon Monoxide under Pressure.* Physical Review Letters, 1998. **81**(10): p. 2092-2095.

47. W. J. Evans, M.J.L., C. S. Yoo, H. Cynn, J. L. Herberg, and R. S. Maxwell, *Pressure-Induced Polymerization of Carbon Monoxide: Disporportionation and Synthiesis of an Energetic Lactonic Polymer.* Chemistry of Materials, 2006. **18**(10): p. 2520-2531.

48. M. Lipp, W.J.E., B. J. Baer, C. S. Yoo, *High-energy-density Extended CO Solid.* Nature Materials, 2005. **4**(3): p. 211-215.

49. Brazhkin, V.V., *Metastable Phases and 'Metastable' Phase Diagrams.* Journal of Physics: Condensed Matter, 2006. **18**(42): p. 9643-9650.

50. McTaggart, F.K., *Reactions of Carbon Monoxide in High-Frequency Discharge.* Australian Journal of Chemistry, 1964. **17**(10): p. 1182-1187.

51. Kennedy, A.F.a.L.A., *Plasma Physics and Engineering*. 2004. New York, NY: Taylor & Francis.

52. Kogelschatz, U., *Dielectric-barrier Discharges: Their History, Discharge Physics, and Industrial Applications.* Plasma Chemistry and Plasma Processing, 2003. **23**(1): p. 1-46.

53. L. H. Reyerson, K.K., *Carbon Suboxide.* Chemical Reviews, 1930. **7**(4): p. 479-492.

54. Mingwang Shao, D.W., Guihua Yu, Bing Hu, Weichao Yu and Yitai Qian, *The Synthesis of Carbon Nanotubes at Low Temperature via Carbon Suboxide Disproportionation* Carbon. 2004. **42**(1): p. 183-185.

55. Porejko, A.B.a.S., *Use of Carbon Suboxide to Obtain Block and Graft Copolymers. I. Grafting of Carbon Suboxide on Polyamide 6.* Journal of Polymer Science Part A-1: Polymer Chemistry, 1970. **8**(9): p. 2491-2500.

56. Porejko, A.B.a.S., *Use of Carbon Suboxide to Obtain Block and Graft Copolymers. II. Grafting of Carbon Suboxide on Polyethylene.* Journal of Polymer Science Part A-1: Polymer Chemistry, 1970. **8**(9): p. 2501-2508.

57. Leonardo Bonsignore, G.L., Daniela Secci, *A Convenient Synthesis of New Heterocycles from Benzimidazoles and Carbon Suboxide.* Journal of Heterocyclic Chemistry, 1992. **29**(4): p. 1033-1034.

58. Leonardo Bonsignorea, F.C., Silvio M. Lavagnab, Giuseppe Loya and Daniela Secci, *Synthesis Via Carbon Suboxide and Pharmaological Activity of Coumarin Derivatives.* Il Farmaco, 1998. **53**(10-11): p. 693-697.

59. Gastone Paiaro, L.P., *The Organometallic Chemistry of Carbon Suboxide.* Comments on modern chemistry. Part A, Comments on inorganic chemistry: a journal of critical discussion of the current literature, 1991. **12**(4): p. 213-235.

60. B. D. Kybett, G.K.J., C. K. Barker, J. L. Margrave, *The Heats of Formation and Polymerization of Carbon Suboxide.* Journal of Physical Chemistry, 1965. **69**(10): p. 3603-3606.

61. Kilpatrick, L.A.M.a.J.E., *Entropy and Related Thermodynamic Properties of Carbon Suboxide.* Journal of Chemical Physics, 1964. **42**(7): p. 2311-2321.

62. Jr., M.W.C., *NIST-JANAF Themochemical Tables, Fourth Edition.* Journal of Physical and Chemical Reference Data Monographs, 1998. **9**: p. 1-1951.

63. John M. Simmie, W.K.M., Henry J. Curran, *Ketene Thermochemistry.* ChemPhysChem, 2008. **9**(5): p. 700-702.

64. Kesler, B.I.L.a.M.G., *A Generalized Thermodynamic Correlation Based on Three-Parameter Corresponding States.* American Institute of Chemical Engineers Journal, 1975. **21**(3): p. 510-527.

65. Jobacka, K.G. and R.C. Reida, *Estimation of Pure-Component Properties from Group-Contributions.* 1987. **57**.

66. Yash Nannoolala, J.R.a.D.R., *Estimation of pure component properties: Part 2. Estimation of critical property data by group contribution.* Fluid Phase Equilibria, 2006.

67. Shapiro, M.M.a.H., *Fundamentals of Engineering Thermodynamics*. 2000: Wiley.

68. McDougall, L.A., *The Entropy and Related Thermodynamic Properties of n-Valeric Acid and Carbon Suboxide and the Determination of the Lowest Bending Frequency of Carbon Suboxide*, in *Physical Chemistry*. 1964, Rice University: Houston, Tx. p. 66.

69. Manson Benedict, G.B.W., and Louis C. Rubin *An Empirical Equation for Thermodynamic Properties of Light Hydrocarbons and Their Mixtures.* Journal of Chemical Physics, 1940. **8**(4): p. 334.

70. Gregory P. Smith, D.M.G., Michael Frenklach, Nigel W. Moriarty, Boris Eiteneer, Mikhail Goldenberg, C. Thomas Bowman, Ronald K. Hanson, Soonho Song, William C. Gardiner, Jr., Vitali V. Lissianski, and Zhiwei Qin. Retrieved May 1, 2009, *http://www.me.berkeley.edu/gri_mech/*.

71. Goodwin D and Moffat H K, Retrieved May 1, 2009, *http://code.google.com/p/cantera/.*

72. Smith, K.M.D.A.a.A.L.S., *Mechanism and Rate of Loss of CO in Glow Discharges in CO, CO-He and CO-N2-He.* Journal of Physics D: Applied Physics, 1977. **10**(3): p. 261-267.

73. Kalyanasundaram, R.H.S.a.A., *Interaction of Carbon Monoxide and Hydrogen Under Silent Discharge: Production of Formaldehyde.* Proceedings Mathematical Sciences, 1947. **27**(5): p. 366-376.

74. M. F. Nagiev, R.M.E.a.I.G.I., Dokl. Akad. Nauk Azerbardyhan SSR, 1958. **14**: p. 347.

75. A. I. Maksimov, L.S.P., A. F. Sergienko, and D. I. Slovetskii, *Investigation of the Stable Products Formed in a Glow Discharge in Carbon Monoxide.* High Energy Chemistry, 1979. **13**(2): p. 136-141.

76. F. Faucitano Martinotti, M.J.W.a.A.P.W., *The Reactivity of Thermal Carbon Atoms in the Gas Phase.* Chemical Communications, 1968. **3**: p. 115-116.

77. Kirsch, D.H.a.L.J., *Reactions of Atomic Carbon C(2^3P_J) by Kinetic Absorption Spectroscopy in the Vacuum Ultra-Violet.* Transactions of the Faraday Society, 1971. **67**: p. 2025-2035.

78. K. H. Becker, R.K., R. Meuser,P. Wiesen,K. D. Bayes, *Kinetics of C2O Radicals Formed in the Photolysis of Carbon Suboxide at 308 and 248 nm.* Journal of Photochemistry and Photobiology A: Chemistry, 1992. **64**: p. 1-14.

79. Haubenstock, N.-L.Y.a.H., *Cyclopolymerization of Carbon Suboxide: Mechanism and Polymer Properties.* Cyclopolymerization and Polymers with Chain-Ring Structures (ACS Symposium Society), 1982. **195**.

80. Palmer, T.J.H.a.H.B., *Kinetics of Deposition of Pyrolytic Carbon Films from Methane and Carbon Suboxide.* Carbon, 1963. **1**: p. 65-70.

81. Bell, L.C.B.a.A.T., *Kinetics of the Oxidation of Carbon Monoxide and the Decomposition of Carbon Dixodie in a Radiofrequency Electric Discharge. II. Theoretical Interpretation.* Ind. Eng. Chem. Fundamen., 1974. **13**(3): p. 210-218.

82. S. F. Mertz, M.C.H., and J. Asmssen, *A Kinetic Model for the Reactions of CO and H2 to CH4 and C2H2 in a Flow Microwave Discharge Reactor.* IEEE Transactions on Plasma Science, 1976. **4**(1): p. 11-23.

83. Cosby, P.C., *Electron-Impact Dissociation of Carbon Monoxide.* J. Chem. Phys., 1992. **98**(10): p. 7804-7818.

84. Kochetov, G.M.G.a.I.V., *Effect of a Small C_3O_2 Additive on the Vibrational Distribution Function of CO Molecules in a Low-Temperature Plasma.* Fizika Plazmy, 2006. **32**(3): p. 273-280.

85. McGrath, T.M.a.W.D., *Flash Photolysis of Carbon Suboxide.* Transactions of the Faraday Society, 1966. **62**: p. 3142-3153.

86. W. Braun, A.M.B., D. D. Davis, and J. D. Simmons, *Flash Photolysis of Carbon Suboxide: Absolue Rate Constants for Reactions of $C(^3P)$ and $C(^1D)$ with H_2, N_2, CO, NO, O_2 and CH_4.* Proceedings of the Royal Society, 1969. **312**(417-434).

87. P. Caubet, G.D., *Origin of C_2 High-Pressure Bands Observed in the Products of a Microwave Discharge through CO.* Chemical Physics Letters, 1993. **218**: p. 529-536.

88. W. D. Geppert, D.R., T. Stoecklin, C. Naulin, M. Costes, D. Chastaing, S. D. Le Picard, I. R. Sims, I. W. M. Smith, *Comparison of the Cross-Sections and Thermal Rate Constants for the Reactions of $C(^3P_j)$ Atoms with O_2 and NO.* Phys. Chem. Chem. Phys., 2000. **2**: p. 2873-2882.

89. A. Fontijn, A.F., A. Ristanovic, M. Y. Randall, J. T. Jankowiak, *CO Chemiluminescence and Kinetics of the C_2 + O_2 Reaction.* J. Phys. Chem. A, 2001. **105**(3182-3189).

90. W. Tsang, R.F.H., *Chemical Kinetic Data Base for Combustion Chemistry. Part I. Methane and Related Compounds.* J. Phys. Chem. Ref. Data, 1986. **15**.

91. W. Bauer, K.H.B., R. Meuser, *Laser Induced Fluorescence Studies on C2O and CH Radicals.* Ber. Bunsenges. Phys. Chem., 1985. **89**.

92. W. B. DeMore, S.P.S., D. M. Golden, R. F. Hampson, M. J. Kurylo, C. J. Howard, A. R. Ravishankara, C. E. Kolb, M. J. Molina, *Chemical Kinetics and Photochemical Data for use in Stratospheric Modeling. Evaluation number 12.* JPL Publication 97-4, 1997: p. 1-266.

93. R. Atkinson, D.L.B., R. A. Cox, J. N. Crowley, R. F. Hampson, R. G. Hynes, M. E. Jenkin, M. J. Rossi, J. Troe, *Evaluated Kinetic and Photochemical Data for Atmospheric Chemistry: Volume I - gas phase reactions of Ox, HOx, NOx and SOx species.* Atmos. Chem. Phys., 2004. **4**: p. 1461-1738.

94. L. M. Arin, P.W., *Reaction of Ozone with Carbon Monoxide.* J. Phys. Chem., 1972. **76**.

95. S. W. Benson, A.E.A.J., *Mechanism of the Gas Phase, Thermal Decomposition of Ozone.* J. Chem. Phys., 1957. **26**: p. 1718-1726.

96. G. Liuti, C.K., S. Dondes, *The Reaction of Carbon Suboxide with Oxygen Atoms and Active Nitrogen.* J. Am. Chem. Soc., 1967. **89**.

97. Jorn Schmedt auf der Gunne, J.B., Wilfried Hoffbauer, and Petra Krieger-Beck, *The Structure of Poly(carbonsuboxide) on the Atomic Scale: A Solid State NMR Study.* Chemistry - A European Journal, 2005. **11**(15): p. 4429-4440.

APPENDIX

Thermodynamic Data

```
units(length = "cm", time = "s", quantity = "mol", act_energy = "cal/mol")

ideal_gas(name = "gas",

      elements = " C  O ",

      species = """ C(gr) C  C2  CO  CO2  C2O  C3O2  O  O2  O3 C3O2(n)""",

      reactions = "all",

      initial_state = state(temperature = 300.0,

                  pressure = OneAtm)     )

#-------------------------------------------------------------------------------

#  Species data

#-------------------------------------------------------------------------------

species(name = "C(gr)",

    atoms = " C:1 ",

    thermo = (

       NASA( [  200.00,  1000.00], [ -3.108720720E-01,   4.403536860E-03,

            1.903941180E-06,  -6.385469660E-09,   2.989642480E-12,
```

```
            -1.086507940E+02,   1.113829530E+00] ),
       NASA( [ 1000.00,  5000.00], [  1.455718290E+00,   1.717022160E-03,
            -6.975627860E-07,   1.352770320E-10,  -9.675906520E-15,
            -6.951388140E+02,  -8.525830330E+00] )
          )
       )
species(name = "C3O2(n)",
   atoms = " C:3  O:2 ",
   thermo = (
      NASA( [  200.00,  1000.00], [ .0024,   0,
             0,  0,   0,
            -27680.6,   .66071] ),
      NASA( [ 1000.00,  5000.00], [  .0024,   0,
             0,  0,   0,
            -27680.6,   .66071] )
          )
      )
```

```
species(name = "C",
   atoms = " C:1 ",
   thermo = (
     NASA( [  200.00,  1000.00], [ 2.554239500E+000, -3.215377200E-004,
           7.337922300E-007, -7.322348700E-010,  2.665214400E-013,
           8.544268100E+004,  4.531308500E+000] ),
     NASA( [ 1000.00,  6000.00], [ 2.605583000E+000, -1.959343400E-004,
           1.067372200E-007, -1.642394000E-011,  8.187058000E-016,
           8.541174200E+004,  4.192386800E+000] )
         ),
   note = "L 7/88"
     )

species(name = "C2",
   atoms = " C:2 ",
   thermo = (
```

```
      NASA( [  200.00,  1000.00], [ 3.693860380E+000, -1.847674270E-003,
            5.237129840E-006, -3.839654010E-009,  8.611357110E-013,
            9.838223180E+004,  2.236770060E+000] ),
      NASA( [ 1000.00,  6000.00], [ 3.252892330E+000,  1.231903070E-003,
           -4.503541560E-007,  7.493566560E-011, -4.579250770E-015,
            9.837373480E+004,  3.958599640E+000] )
          ),
   note = "singlet T05/09"
      )

species(name = "CO",
   atoms = " C:1  O:1 ",
   thermo = (
      NASA( [  200.00,  1000.00], [ 3.579533500E+000, -6.103536900E-004,
            1.016814300E-006,  9.070058600E-010, -9.044244900E-013,
           -1.434408600E+004,  3.508409300E+000] ),
      NASA( [ 1000.00,  6000.00], [ 3.048485900E+000,  1.351728100E-003,
```

```
            -4.857940500E-007,  7.885364400E-011, -4.698074600E-015,
            -1.426611700E+004,  6.017097700E+000] )
           ),
    note = "RUS 79"
      )

species(name = "CO2",
    atoms = " C:1  O:2 ",
    thermo = (
      NASA( [  200.00,  1000.00], [ 2.356813000E+000,  8.984129900E-003,
            -7.122063200E-006,  2.457300800E-009, -1.428854800E-013,
            -4.837197100E+004,  9.900903500E+000] ),
      NASA( [ 1000.00,  6000.00], [ 4.636511100E+000,  2.741456900E-003,
            -9.958975900E-007,  1.603866600E-010, -9.161985700E-015,
            -4.902490400E+004, -1.934895500E+000] )
           ),
    note = "L 7/88"
```

```
      )


species(name = "C2O",
   atoms = " C:2  O:1 ",
   thermo = (
     NASA( [  200.00,  1000.00], [ 2.862782140E+000,  1.197012040E-002,
           -1.808512220E-005,  1.527777300E-008, -5.200631630E-012,
            4.513284920E+004,  8.897590990E+000] ),
     NASA( [ 1000.00,  5000.00], [ 5.424683780E+000,  1.853939450E-003,
           -5.179329560E-007,  6.776462300E-011, -3.533152370E-015,
            4.453639070E+004, -3.696084050E+000] )
          ),
   note = "T 7/08"
     )


species(name = "C3O2",
   atoms = " C:3  O:2 ",
```

```
    thermo = (
      NASA( [  200.00,  1000.00], [ 2.196694900E+000,  3.145519000E-002,
            -5.074552200E-005,  4.357903800E-008, -1.473501400E-011,
            -1.294609900E+004,  1.329847900E+001] ),
      NASA( [ 1000.00,  6000.00], [ 8.461749400E+000,  4.815529600E-003,
            -1.809306700E-006,  3.007864200E-010, -1.837213700E-014,
            -1.432716000E+004, -1.706050800E+001] )
           ),
    note = "L 7/88"
      )


species(name = "O",
    atoms = " O:1 ",
    thermo = (
      NASA( [  200.00,  1000.00], [ 3.168267100E+000, -3.279318840E-003,
            6.643063960E-006, -6.128066240E-009,  2.112659710E-012,
            2.912225920E+004,  2.051933460E+000] ),
```

```
      NASA( [ 1000.00,  6000.00], [ 2.543636970E+000, -2.731624860E-005,
            -4.190295200E-009,  4.954818450E-012, -4.795536940E-016,
             2.922601200E+004,  4.922294570E+000] )
           ),
    note = "L 1/90"
      )

species(name = "O2",
    atoms = " O:2 ",
    thermo = (
      NASA( [  200.00,  1000.00], [ 3.782456360E+000, -2.996734150E-003,
             9.847302000E-006, -9.681295080E-009,  3.243728360E-012,
            -1.063943560E+003,  3.657675730E+000] ),
      NASA( [ 1000.00,  6000.00], [ 3.660960830E+000,  6.563655230E-004,
            -1.411494850E-007,  2.057976580E-011, -1.299132480E-015,
            -1.215977250E+003,  3.415361840E+000] )
           ),
```

```
    note = "REF ELEMENT RUS 89"
      )

species(name = "O3",
    atoms = " O:3 ",
    thermo = (
      NASA( [  200.00,  1000.00], [ 3.407382210E+000,  2.053790630E-003,
            1.384860520E-005, -2.233115420E-008,  9.760732260E-012,
            1.586449790E+004,  8.282475800E+000] ),
      NASA( [ 1000.00,  6000.00], [ 1.233029140E+001, -1.193247830E-002,
            7.987412780E-006, -1.771945520E-009,  1.260758240E-013,
            1.267558310E+004, -4.088233740E+001] )
          ),
    note = "L 5/90"
      )
```

Modeling Emission Spectra

```
%%%% Carbon Monoxide Spectra %%%%
clc
close all
clear

%%%%%%%%%%%%%%%%%%%%%%

%Parameters

%%%%%%%%%%%%%%%%%%%%%%

Tel = 10000; %K
Tvib = 1000; %K
Trot = 400; %K
FWHM = 0.1; %nm
showstates = 1;

%%%%%%%%%%%%%%%%%%%%%%

%Universal Constants

%%%%%%%%%%%%%%%%%%%%%%

k_b=1.3806503e-23;          %m2 kg s-2 K-1
h = 6.626068e-34; %m^2*kg/s
c = 300e6;         %m/s
jev=1.609e-19;  %J/eV

%%%%%%%%%%%%%%%%%%%%%%

%Molecular Constants

%%%%%%%%%%%%%%%%%%%%%%

zp = h.*c.*([753.49, 1072, 1086].*100); %Zero Point difference (De-Do)
diss = h*c*89460*100;   %Dissociation Energy from Ground State
Te = h.*c.*[(65074.6*100), (86928*100), (91915*100)]; %Energy at zp
relative to ground
bot = h.*c.*(90542*100);    %Ground State energy at bottom of well
meff = (12*16)/(12+16)/6.022e23/1000; %kg
k = [927.9, 1751, 1919.6]; %N/m
w = (k./meff).^(0.5); %1/s
Be = h.*c.*([1.6116 1.961 1.9536].*100); %J
alpha = [0.02229 0.027 0.020];

titl={'A1Pi';'B1Sig';'C1Sig'}s;

%%%%%%%%%%%%%%%%%%%%%%%%
```

```
%%% Spec for comparison

%%%%%%%%%%%%%%%%%%%%%%%%%

spec=dlmread('CO_full_spectrum_300-650_batch_afterlunch.csv');
swan=dlmread('C2Swan_FitSpectra_CO_full_spectrum_300-
650_batch_afterlunch.csv');

w_exp=spec(:,2)-.3;
i_exp_raw=-spec(:,3);
bg=mean(i_exp_raw(w_exp>610&w_exp<630));
i_exp=i_exp_raw-bg;
i_exp=i_exp/max(i_exp(w_exp>440&w_exp<460));

mn=max(find(swan(:,1)<3000));
mx=max(find(swan(:,1)<6500));

w_swan=swan(mn:mx,1)./10;
i_swan=swan(mn:mx,3);

%%%%%%%%%%%%%%%%%%%

%Calculate states

%%%%%%%%%%%%%%%%%%%

v_tild = h.*c./(1./([1518.2, 2112.7, 2175.92].*100)); %[A1Pi, B1Sig,
C1Sig]
v_tild_xe = h.*c./(1./([19.4, 15.22, 14.76].*100)); %[A1Pi, B1Sig,
C1Sig]
cont = 1;

fc_angs = {[0.08898 0.18159 0.21056 0.18339 0.13399 0.08706 0.06211
0.20941 0.01591 0.00835 0.00429 0.00217 0.00109 0.00055],[0.25053
0.17569 0.03039 0.00420 0.05214 0.09553 0.10665 0.09311 0.07008 0.04781
0.03046 0.01849 0.01085]};
fc_herz = {[0.072 0.165 0.214],[0.211 0.192 0.031],[0.293 0.034]};

v_angs = {[0:size(fc_angs{1},2)-1],[0:size(fc_angs{2},2)-1]};
v_herz = {[0:size(fc_herz{1},2)-1],[0:size(fc_herz{2},2)-
1],[0:size(fc_herz{3},2)-1]};

%%%%%%%%%%%%%%%%%%%%%%%%%%%

%Calculate Energy of States

%%%%%%%%%%%%%%%%%%%%%%%%%%%

jmax = 100;
```

```
%%STATE A%%
v=0;
for q=1:length(v_angs{1})
    G_A(q) = ((v+1/2)*v_tild(1)-(v+1/2)^2*v_tild_xe(1))+Te(1);
    D_A(q) = 4*Be(1)^3/(G_A(q))^2; %J
    for j = 1:jmax
        J=j-1;
        F_A(q,j) = Be(1)*J*(J+1)-D_A(q)*J^2*(J+1)^2;
        S_A(q,j) = G_A(q) + F_A(q,j);
    end
    v = v + 1;
end

%%STATE B%%
v=0;
for t=1:length(v_angs)
    G_B(t) = ((v+1/2)*v_tild(2)-(v+1/2)^2*v_tild_xe(2))+Te(2);
    D_B(t) = 4*Be(2)^3/(G_B(t))^2; %J
    for j = 1:jmax
        J=j-1;
        F_B(t,j) = Be(2)*J*(J+1)-D_B(t)*J^2*(J+1)^2;
        S_B(t,j) = G_B(t) + F_B(t,j);

E_B(t,j)=(Te(2)/(k_b*Tel)+G_B(t)/(k_b*Tvib)+F_B(t,j)/(k_b*Trot));
        Nu_B(t,j)=((2*J)+1)*exp(-E_B(t,j));
    end
    v = v + 1;
end

%%STATE C%%
v=0;
for u=1:length(v_herz)
    G_C(u) = ((v+1/2)*v_tild(3)-(v+1/2)^2*v_tild_xe(3))+Te(3);
    D_C(u) = 4*Be(3)^3/(G_C(u))^2; %J
    for j = 1:jmax
        J=j-1;
        F_C(u,j) = Be(3)*J*(J+1)-D_C(u)*J^2*(J+1)^2;
        S_C(u,j) = G_C(u) + F_C(u,j);

E_C(u,j)=(Te(3)/(k_b*Tel)+G_C(u)/(k_b*Tvib)+F_C(u,j)/(k_b*Trot));
        Nu_C(u,j)=((2*J)+1)*exp(-E_C(u,j));
    end
    v = v + 1;
end

%%%%%%%%%%%%%%%%%%%%%%%%%

%Calcuate Angstrom Bands

%%%%%%%%%%%%%%%%%%%%%%%%%
```

```
for t = 1:length(v_angs)
    for q = 1:length(v_angs{t})
        for j=1:jmax
            E_up_a = S_B(t,j);
            if j>1
                E_low_P_a = S_A(q,j-1);
            else
                E_low_P_a = NaN;
            end
            E_low_Q_a = S_A(q,j);
            if j==jmax
                E_low_R_a = NaN;
            else
                E_low_R_a = S_A(q,j+1);
            end
            DeltaE_P_a(t,q,j) = (E_up_a-E_low_P_a); % J
            DeltaE_Q_a(t,q,j) = (E_up_a-E_low_Q_a);
            DeltaE_R_a(t,q,j) = (E_up_a-E_low_R_a);
            HLF_a = 1;
            Otherfactors_a = 1/(2*j+1);
            Int_P_a(t,q,j) =
Nu_B(t,j)*fc_angs{t}(q)*DeltaE_P_a(t,q,j)^4*HLF_a*Otherfactors_a; %arb
units
            Int_Q_a(t,q,j) =
Nu_B(t,j)*fc_angs{t}(q)*DeltaE_Q_a(t,q,j)^4*HLF_a*Otherfactors_a;
            Int_R_a(t,q,j) =
Nu_B(t,j)*fc_angs{t}(q)*DeltaE_R_a(t,q,j)^4*HLF_a*Otherfactors_a;

            del_G_angs{t,q} = G_B(t) - G_A(q);
        end
    end
end

[I_angs, W_angs] = specsort(DeltaE_P_a,DeltaE_Q_a,DeltaE_R_a, Int_P_a,
Int_Q_a, Int_R_a, FWHM);

%plot(Wave3,I_conv,Wave3,Int3,Wave2,I2) %% check convolution and FWHM
% figure
% plot(W_angs,I_angs)


%%%%%%%%%%%%%%%%%%%%%%%%%%%%%

%Calcuate Herzberg Bands

%%%%%%%%%%%%%%%%%%%%%%%%%%%%%

for t = 1:length(v_herz)
    for q = 1:length(v_herz{t})
        for j=1:jmax
            E_up_h = S_C(t,j);
            if j>1
```

```
                E_low_P_h = S_A(q,j-1);
            else
                E_low_P_h = NaN;
            end
            E_low_Q_h = S_A(q,j);
            if j==jmax
                E_low_R_h = NaN;
            else
                E_low_R_h = S_A(q,j+1);
            end
            DeltaE_P_h(t,q,j) = (E_up_h-E_low_P_h); % J
            DeltaE_Q_h(t,q,j) = (E_up_h-E_low_Q_h);
            DeltaE_R_h(t,q,j) = (E_up_h-E_low_R_h);
            HLF_h = 1;
            Otherfactors_h = 1/(2*j+1);
            Int_P_h(t,q,j) =
Nu_C(t,j)*fc_herz{t}(q)*DeltaE_P_h(t,q,j)^4*HLF_h*Otherfactors_h; %arb
units
            Int_Q_h(t,q,j) =
Nu_C(t,j)*fc_herz{t}(q)*DeltaE_Q_h(t,q,j)^4*HLF_h*Otherfactors_h;
            Int_R_h(t,q,j) =
Nu_C(t,j)*fc_herz{t}(q)*DeltaE_R_h(t,q,j)^4*HLF_h*Otherfactors_h;

            del_G_herz{t,q} = G_C(t) - G_A(q);
        end
    end
end

[I_herz, W_herz] = specsort(DeltaE_P_h,DeltaE_Q_h,DeltaE_R_h, Int_P_h,
Int_Q_h, Int_R_h, FWHM);

%plot(Wave3,I_conv,Wave3,Int3,Wave2,I2) %% check convolution and FWHM
% figure
% plot(W_herz,I_herz)

figure
plot(W_herz,0.3*I_herz,W_angs,I_angs,w_swan+10.2,i_swan)
hold on
plot(w_exp+11,i_exp,'-g')

legend('Herzberg','Angstrom','Swan','Experimental')
%%%%%%%%%%%%%%%%%%%%%%%%%%%%%

%Show wells of the states

%%%%%%%%%%%%%%%%%%%%%%%%%%%%%

Re = [1.2353, 1.1197, 1.1219].*1e-10; %[A1Pi, B1Sig, C1Sig] m
R= linspace(.8e-10,3*Re(1),100); % m

%Estimate the dissociation energy for states B and C
```

```
%B first
v=0;
for t=1:10
    x(t) = v + 1/2;
    G_B_tmp(t) = ((v+1/2)*v_tild(2)-(v+1/2)^2*v_tild_xe(2))+Te(2);
    v = v + 1;
end
slp = diff(G_B_tmp);
yy = polyfit(x(1:end-1),slp,1);
Do_B = -0.5*(yy(2)/yy(1)-0.5)*yy(2);
De_B = Do_B+zp(2);

%C second
v=0;
for t=1:10
    x(t) = v + 1/2;
    G_C_tmp(t) = ((v+1/2)*v_tild(3)-(v+1/2)^2*v_tild_xe(3))+Te(3);
    v = v + 1;
end
slp = diff(G_C_tmp);
yy = polyfit(x(1:end-1),slp,1);
Do_C = -0.5*(yy(2)/yy(1)-0.5)*yy(2);
De_C = Do_C+zp(3);


De = [(25601*100),De_B/(h*c),De_C/(h*c)];   %[A1Pi, B1Sig, C1Sig] J
vmax = h*c*De;
for l=1:length(k)
    a(l) = ((meff.*w(l).^2)./(2.*h.*c.*De(l))).^(0.5); %1/m
end


if showstates
figure
    for j = 1: length(De)
        V{j} = h.*c.*De(j).*(1-exp(-a(j).*(R-
Re(j)))).^2./jev+Te(j)./jev;

        plot(R./1e-10,V{j})
        hold on
    end

xlim([0.5,2.5])
ylim([8,13])

xlabel('r (Angstrom)')
ylabel('Energy (eV)')

%Plot Vibrational Energy Levels
eng = {G_A,G_B,G_C};
for yy=1:3
```

```
R_right = Re(yy)/1e-10+(-log(1-sqrt((eng{yy}-
Te(yy))./(h*c*De(yy))))/a(yy))./1e-10;
R_left = Re(yy)/1e-10+(-log(1+sqrt((eng{yy}-
Te(yy))./(h*c*De(yy))))/a(yy))./1e-10;
line([R_left;R_right],[eng{yy}./jev;eng{yy}./jev],'Color','b')
end

X = [Re(3)/1e-10 Re(3)/1e-10];
Y = [Te(3)/jev h.*c.*De(1).*(1-exp(-a(1).*(Re(3)-
Re(1)))).^2./jev+Te(1)./jev];
line(X,Y)
end
```

Additional Functions:

```
function [I,W] = specsort(DeltaE_P,DeltaE_Q,DeltaE_R,Int_P, Int_Q,
Int_R, FWHM)

h = 6.626068e-34; %m^2*kg/s
c = 300e6;        %m/s

Lambda_P =(h*c./DeltaE_P);
Lambda_Q =(h*c./DeltaE_Q);
Lambda_R =(h*c./DeltaE_R);

W_P = reshape(Lambda_P,prod(size(Lambda_P)),1);
W_Q = reshape(Lambda_Q,prod(size(Lambda_P)),1);
W_R = reshape(Lambda_R,prod(size(Lambda_P)),1);
I_P = reshape(Int_P,prod(size(Lambda_P)),1);
I_Q = reshape(Int_Q,prod(size(Lambda_P)),1);
I_R = reshape(Int_R,prod(size(Lambda_P)),1);
W_all = [W_P;W_Q;W_R]*1e9; % nm units
I_all = [I_P;I_Q;I_R];

I_P(isnan(I_P))=0; %% Correct for unallowable DeltaJ=-1 from J=1 state.

Wave = linspace(min(W_all),max(W_all),1e5);
I = Wave*0;
Wave1 = [Wave';W_all];
I1 = [I';I_all];
[Wave2,ind] = sort(Wave1);
I2 = I1(ind);
%plot(Wave2,I2)

%Incorporate broadening effects

DW3 = 5e-2;
Wave3 = [300:DW3:650];
```

```
%Increase resolution
for i=1:length(Wave3)
    Int3(i) = sum(I2((Wave2>(Wave3(i)-
DW3/2))&(Wave2<=(Wave3(i)+DW3/2))));
end

%Convolution with slit function

W_slit = [-10:DW3:10];
sigma = FWHM/(2*sqrt(2*log(2)));
I_slit = exp(-W_slit.^2/(2*sigma^2));

I_conv = fastconv(Int3,I_slit);
I = I_conv./max(I_conv);
W = Wave3;

function [y]=fastconv(x, h)
%FCONV Fast Convolution
%   [y] = FCONV(x, h) convolves x and h, and normalizes the output
%         to +-1.
%
%      x = input vector
%      h = input vector
%
%      See also CONV
%
%   NOTES:
%
%   1) I have a short article explaining what a convolution is.  It
%      is available at http://stevem.us/fconv.html.
%
%
%Version 1.0
%Coded by: Stephen G. McGovern, 2003-2004.

Ly=length(x)+length(h)-1;  %
Ly2=pow2(nextpow2(Ly));    % Find smallest power of 2 that is > Ly
X=fft(x, Ly2);         % Fast Fourier transform
H=fft(h, Ly2);             % Fast Fourier transform
Y=X.*H;                    %
y=real(ifft(Y, Ly2));      % Inverse fast Fourier transform
y=y(1:1:length(x));              % Take just the first length(x)
%y=y/max(abs(y));           % Normalize the output
```